NSG - 646

EES SERIES REPORT NO. 5

REPORTS ON

HYBRID ANALOG-DIGITAL TECHNIQUES AND RANDOM-PROCESS STUDIES

1964-1965

ENGINEERING EXPERIMENT STATION
COLLEGE OF ENGINEERING
THE UNIVERSITY OF ARIZONA, TUCSON

EES SERIES REPORT NO. 5

Reports On

HYBRID ANALOG-DIGITAL TECHNIQUES AND RANDOM-PROCESS STUDIES

1964 - 1965

Acknowledgment

The permission of the editor and publisher of SIMULATION to reprint this material in the public interest is gratefully acknowledged.

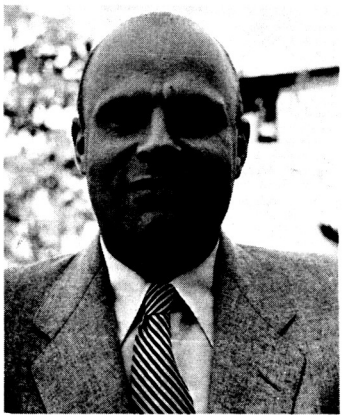

Hybrid-Computer Techniques for Measuring Statistics from Quantized Data

by

GRANINO A. KORN
The University of Arizona

GRANINO ARTHUR KORN was born in 1922 in Berlin, Germany. He graduated from Brown University in 1942 and obtained M.A. and Ph.D. degrees in physics from Columbia and Brown in 1943 and 1948, respectively. After wartime service in the United States Navy, Dr. Korn was successively a project engineer with Sperry Gyroscope, head of the analysis group at Curtiss-Wright/Columbus, a staff engineer with Lockheed/Burbank, and a consultant under his own name. Since 1957, he has been a professor of Electrical Engineering at the University of Arizona in Tucson, where he teaches courses on electronic computers and communications theory.

Together with his wife, Theresa M. Korn, Dr. Korn is the author of *Electronic Analog Computers* (1952 and 1956), *Mathematical Handbook for Scientists and Engineers* (1961), and *Electronic Analog and Hybrid Computers* (1964); due in 1965 are *Random-process Simulation and Control* and *Basic Tables for Electrical Engineering*. Dr. Korn is co-editor-in-chief of the McGraw-Hill *Computer Handbook* (1961) and the *Digital Computer User's Handbook* (in print), has contributed articles to seven other engineering handbooks, and edits McGraw-Hill's new series of short numerical tables.

Dr. Korn has taught in Mexico and surveyed engineering education in Chile as a consultant to the National Academy of Sciences. He is a member of Sigma Xi, Simulation Councils, Inc., and the International Analog Computer Association.

As Chairman of the Editorial Board of SIMULATION Granino Korn was "Presented" in the April 1964 issue of our Journal with a somewhat different biographical sketch.

ABSTRACT

Digital data processing necessarily involves quantization *(roundoff) of input data. The statistical theory of amplitude quantization indicates that the effects of quantization on* statistics *are often negligible or can be approximately predicted and corrected, even with surprisingly coarse quantization. This tutorial paper reviews contributions to the theory made in England, the Netherlands, and Russia, as well as B. Widrow's original work in this country. Applications to remarkably inexpensive hybrid analog-digital averaging computers and correlators are also discussed. The theory can pay very handsome practical dividends: in many applications, 2- to 4-bit analog-to-digital converters and data-transmission channels can yield averages, mean squares, and correlation functions with 10- to 20-bit accuracy, and one-bit (polarity-coincidence) correlators are often practical.*

STATISTICAL EFFECTS OF QUANTIZATION

1. Introduction.

Digital data processing necessarily involves quantization (roundoff, grouping) of input data samples. The range of each random variable, say x, is subdivided into *class intervals*

$$i\Delta x - \frac{\Delta x}{2} < x \leq i\Delta x + \frac{\Delta x}{2} \quad (i = 0, \pm 1, \pm 2, \cdots)$$

of equal width Δx. The quantization operation replaces each value of x by the nearest class-interval center $i\Delta x$ (Figure 1a). The quantizer output x_Q can be regarded as the sum of the input x and a roundoff error

$$n_Q = x_Q - x \tag{1}$$

$n_Q = n_Q(t)$ is referred to as *quantization noise*, although the "noise" n_Q is definitely (not just stochastically) determined if x is known (Figure 1b). If statistics, such as averages or correlation estimates, are computed

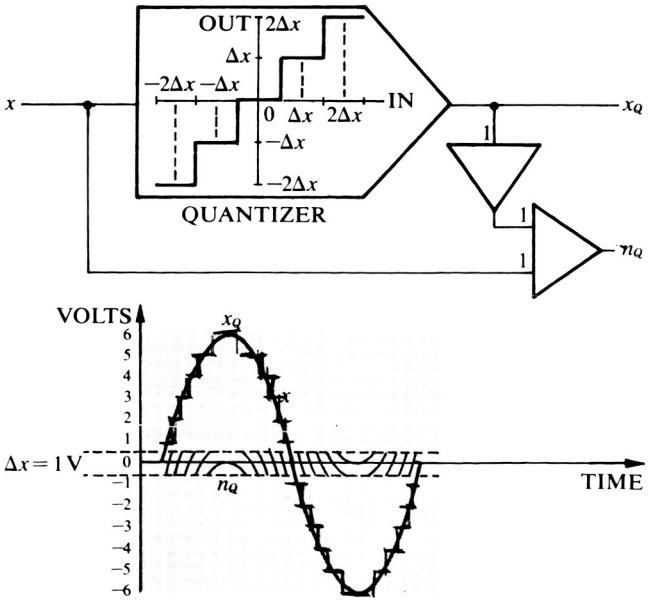

Figure 1 – Demonstration of amplitude quantization (a) and quantizer input, output, and quantization noise for sinusoidal input (b).

from quantized data, the roundoff will increase estimate variances and may also affect (bias) the mean of the estimate. For an important class of random processes, however, theoretical study yields the highly practical result that *the biasing effects of quantization average out approximately or can be approximately predicted and corrected, even with surprisingly coarse quantization.* A quantitative hold on this phenomenon will permit us to realize the most remarkable savings in analog-to-digital conversion and digital data transmission and storage. Computation of 13-bit estimates of mean values, mean squares, and correlation functions will rarely require conversion, transmission, and/or storage of over eight bits, and four bits or less is often sufficient. Digital computation of 13-bit estimates will then require 13-bit output, but at most 8-bit inputs.

The statistical theory of amplitude quantization, due essentially to B. Widrow,[1,16 to 18] will be reviewed in sections 8 to 12. We will, however, begin by simply stating the principal results (sections 3 and 4) and then demonstrate their practical application (sections 5 to 7) before we present any theoretical derivation.

2. Characteristic Functions.

For all random variables u, v (continuous, discrete, or otherwise), we can introduce *characteristic functions*

$$\chi_u(q) = E\{e^{jqu}\} \quad \chi_{u,v}(q_1, q_2) = E\{e^{j(q_1 u + q_2 v)}\} \tag{2}$$

Each characteristic function uniquely defines the corresponding probability distribution.[2] Series expansion of the exponential yields

$$\chi_u(q) = 1 + jqE\{u\} - \frac{1}{2}q^2 E\{u^2\} + \cdots$$

$$\chi_{u,v}(q_1, q_2) = 1 + jq_1 E\{u\} + jq_2 E\{v\} - \frac{1}{2}q_1^2 E\{u^2\} - \frac{1}{2}q_2^2 E\{v^2\} - q_1 q_2 E\{uv\} + \cdots \tag{3}$$

for all real q, q_1, q_2 whenever the expected values (moments) on the right exist. It follows that $\chi_u(0) = \chi_{u,v}(0, 0) = 1$, and

$$E\{u^m\} = j^{-m}\left[\frac{d^m \chi_u}{dq^m}\right]_{q=0}$$

$$E\{u^m v^n\} = j^{-(m+n)}\left[\frac{\partial^{m+n}\chi_{u,v}}{\partial^m q_1 \partial^n q_2}\right]_{q_1 = q_2 = 0} \tag{4}$$

If u and v are statistically independent random variables, then

$$\chi_{u,v}(q_1, q_2) = \chi_u(q_1)\chi_v(q_2)$$

$$\chi_{u+v}(q) = \chi_u(q)\chi_v(q)$$

Conversely, the first relation implies statistical independence, but the second one does not necessarily do so.

3. The Quantizing Theorems and Sheppard's Corrections.

We now state the principal results of the statistical theory of amplitude quantization,[1,16 to 18] reserving the proofs for sections 8 and 9.

a. If the probability density $p(x)$ of our input x is "band-limited" so that its characteristic function $\chi_x(q) \equiv E\{e^{jqx}\}$ vanishes for $|q| \geq 2\pi/\Delta x - \epsilon$ $(\epsilon > 0)$, then every existing mean value (moment) $E\{x^m\}$ $(m = 1, 2, \cdots)$ is completely determined by moments of the quantizer output x_Q, and the first-order probability distribution of the quantization noise n_Q is uniform between $-\Delta x/2$ and $\Delta x/2$.

b. If the joint probability density $p(x, y)$ of two input variables x, y is "band-limited" so that the joint characteristic function $\chi_{x,y}(q_1, q_2)$ $E\{e^{j(q_1 x + q_2 y)}\}$ is zero for $|q_1| \geq 2\pi/\Delta x - \epsilon$, $q_2 \geq 2\pi/\Delta y - \epsilon$ $(\epsilon > 0)$, then every existing moment $E\{x^m y^n\}$ $(m, n = 1, 2, \cdots)$ is completely determined by joint moments of the quantizer outputs x_Q, y_Q, and quantization noise samples $n_{Qx} = x_Q - x$, $n_{Qy} = y_Q - y$ are uniformly distributed and statistically independent.

More specifically, we shall prove in section 9 that the conditions of theorem 1 imply

$$\left.\begin{aligned} E\{x\} &= E\{x_Q\} \\ E\{x^2\} &= E\{x_Q^2\} - \frac{1}{12}(\Delta x)^2 \\ E\{x^4\} &= E\{x_Q^4\} - \frac{1}{2}(\Delta x)^2 E\{x_Q^2\} + O\left[(\Delta x)^4\right] \end{aligned}\right\} \tag{6}$$

and hence

$$\begin{aligned} \mathrm{Var}\{x_Q\} &= \mathrm{Var}\{x\} + \frac{1}{12}(\Delta x)^2 \\ \mathrm{Var}\{x_Q^2\} &= \mathrm{Var}\{x^2\} + \frac{1}{3}(\Delta x)^2 E\{x^2\} + O\left[(\Delta x)^4\right] \end{aligned} \tag{7}$$

whenever the expected values in question exist. Relations of this type have been known for many years as *Sheppard's corrections for grouped data;*[3] Widrow's theory furnishes a more general and rigorous justification for these formulas.

Similarly, the conditions of theorem 2 imply

$$E\{xy\} = E\{x_Q y_Q\} \quad (x \neq y) \tag{8}$$

and hence, if we let $x = x(t_1)$ and $y = x(t_2)$ or $y(t_2)$,

$$R_{xx}(t_1, t_2) = \begin{cases} E\{x_Q^2(t_1)\} - \frac{1}{12}(\Delta x)^2 & (t_1 = t_2) \\ R_{x_Q x_Q}(t_1, t_2) & (t_1 \neq t_2) \end{cases} \tag{9}$$

$$R_{xy}(t_1, t_2) = R_{x_Q y_Q}(t_1, t_2) \qquad (x \neq y) \tag{10}$$

Finally,

c. If the probability distribution of x is "band-limited" so that $\chi_x(q) = 0$ for $|q| \geq \pi/\Delta x$, then the probability distribution of x is *completely determined* by that of the quantizer output x_Q. An analogous theorem holds for the joint distribution of two quantizer inputs (section 9).

HYBRID ANALOG-DIGITAL MEASUREMENTS EMPLOYING COARSE QUANTIZATION

4. Gaussian or Approximately Gaussian Data.

If the appropriate quantizing theorems apply, equations (6) to (10) indicate that the effects of even relatively coarse quantization on *statistics* are either negligible or easily corrected. Actually, real random data cannot possibly satisfy the conditions of section 3 *exactly,* since physical signals are necessarily bounded; for continuous $x(t)$, moreover, statistical independence of $n_Q(t_1), n_Q(t_2)$ for arbitrarily small $\tau = t_2 - t_1$ would imply infinite signal power.[1,16] Nevertheless, many real signals satisfy the quantizing theorems so nearly that excellent approximations result, and the errors of such approximations can be neatly predicted by the relations of section 9.

For the important case of *Gaussian data,* Table 1 and Figure 2 summarize the most important results and indicate that *quantization* errors in measurements of $E\{x\}$, $E\{x^2\}$, *and* $R_{xx}(\tau)$ for *Gaussian processes are either negligible or easily corrected, even with class intervals* Δx *as large as* 3σ.

5. Simplified Correlators

Hybrid analog-digital techniques involving coarse quantization are especially fruitful for correlation measurements, for we may be able to replace relatively expensive analog delay and multiplier circuits by simple digital circuits. With Gaussian (or approximately Gaussian) signals, three-bit-plus-sign conversion and delay circuits can feed a simple digital or hybrid multiplier/accumulator to produce excellent correlation estimates in many practical applications.[1,4,5,17,20 to 26]

Even one-bit correlators, which merely average sgn $x(t_1)$ sgn $y(t_2)$ with the simplest of digital circuitry (Figure 3a), can be very useful. *For Gaussian data with zero mean,* in particular, the one-bit correlation function is simply related to the true correlation function $R_{xy}(t_1, t_2)$:[6]

$$E\{\operatorname{sgn} x(t_1)\ \operatorname{sgn} y(t_2)\} = \frac{2}{\pi} \arcsin \frac{R_{xy}(t_1, t_2)}{\sqrt{E\{x^2(t_1)\}\, E\{y^2(t_2)\}}} \tag{11}$$

Similar formulas have been derived for autocorrelation and cross-correlation of known signals with additive Gaussian noise.[1,4,7 to 11,23] One-bit correlators are especially inexpensive and reliable, since they require only comparators and digital circuitry. One-bit correlators can replace true correlators in many testing, detection and process-measurement applications: Widrow,[1] for instance, applied one-bit correlation to recorded radar returns from the planet Venus and obtained practically unequivocal detection in over 40 db of noise.

Δx	$\sigma = \sqrt{\text{Var}\{x\}}$	2σ	3σ
$\max \lvert E\{x_Q\} - E\{x\}\rvert$ if $E\{x\} \neq 0$	$8.3 \times 10^{-10} \Delta x$	$2.3 \times 10^{-3} \Delta x$	$3.5 \times 10^{-2} \Delta x$
$\text{Var}\{x_Q\} - \text{Var}\{x\} - \frac{(\Delta x)^2}{12}$ $(E\{x\} = 0)$	$-1.1 \times 10^{-8} \sigma^2$	$-3.1 \times 10^{-2} \sigma^2$	$-0.54\sigma^2$
$E\{n_Q^2\} - \frac{(\Delta x)^2}{12}$ $(E\{x\} = 0)$	$-2.6 \times 10^{-10} (\Delta x)^2$	$-7.2 \times 10^{-4} (\Delta x)^2$	$-1.1 \times 10^{-2} (\Delta x)^2$

Table 1 – Errors Resulting from Application of Equations (6) and (7) to Gaussian Processes (Data from reference 1)

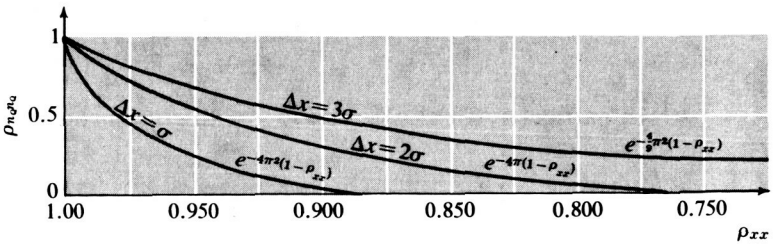

Figure 2 – Normalized autocorrelation function of quantization noise, $\rho_{n_Q n_Q} \approx \rho_{x_Q x_Q} - \rho_{xx}$ versus ρ_{xx} for stationary Gaussian $x(t)$, where

$$\rho_{uu}(\tau) = \frac{R_{uu}(\tau) - [E\{u\}]^2}{E\{u^2\} - [E\{u\}]^2}$$

(based on reference 1).

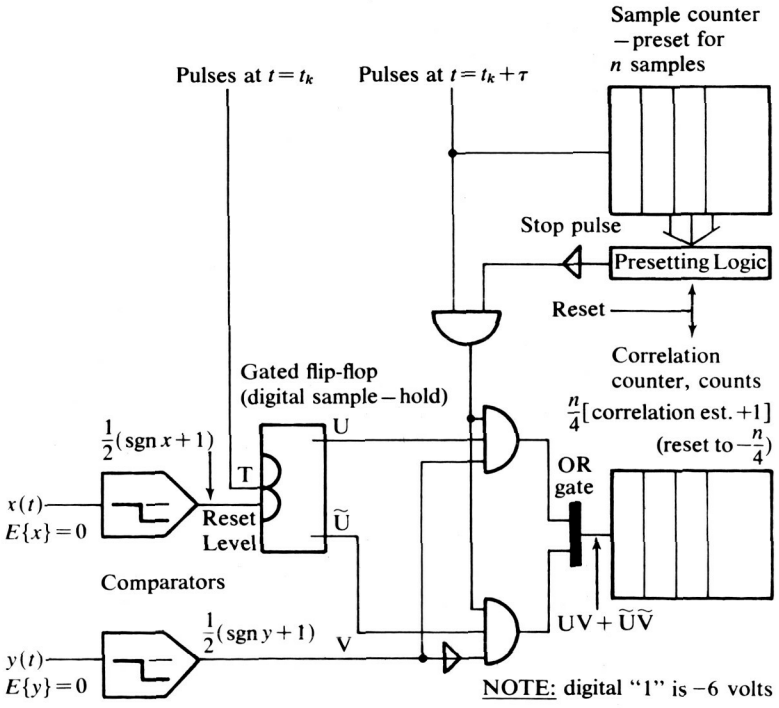

Figure 3a – Approximate correlation employing one-bit quantization of x and y

As a somewhat less radical measure, we can correlate $x_Q(t_1)$ with $y(t_2)$, *i.e.*, we quantize only one of the two correlator input signals. This still permits digital delay, and multiplication is conveniently accomplished with a simple D/A converter whose reference input is replaced by $y(t_2)$. The simplest correlators of this type employ one-bit quantization of $x(t_1)$, *i.e.*, they average $y(t_2)\,\mathrm{sgn}\,x(t_1)$; this permits hybrid multiplication by a simple analog switch (Figure 3b). *For Gaussian signals with zero mean,* the resulting estimates are simply proportional to true correlation estimates:[11,17]

$$E\{y(t_2)\,\mathrm{sgn}\,x(t_1)\} = \frac{E\{|x(t_1)|\}}{\sqrt{E\{x^2(t_1)\}}}\,\frac{R_{xy}(t_1,t_2)}{\sqrt{E\{x^2(t_1)\}}} \tag{12}$$

$$= \sqrt{\frac{2}{\pi}}\,\frac{R_{xy}(t_1,t_2)}{\sqrt{E\{x^2(t_1)\}}}$$

In particular, for any Gaussian x with zero mean,

$$E\{x\,\mathrm{sgn}\,x\} = E\{|x|\} = \sqrt{\frac{2}{\pi}}\sqrt{E\{x^2\}} \tag{13}$$

which permits us to measure the mean square of a Gaussian signal by its mean absolute value, which is usually easier to compute.

6. Use of Dither.[1,12,24]

Given any random variable s_x which satisfies the first or second quantizing theorem of section 3, the same holds for the sum $x+s_x$ of s_x and every random variable x statistically independent of s_x, since

$$\chi_{s_x}(q) = \chi_x(q)\chi_{s_x}(q) \tag{14}$$

(section 2). Even if s_x satisfies

$$\chi_{x+s_x}(q) = 0 \quad \left(|q| \geq \frac{2\pi}{\Delta x}\right) \tag{15}$$

only approximately, $x+s_x$ will also satisfy the quantizing theorem approximately.

We can, therefore, greatly extend the applicability of coarse-quantization estimates by adding *dither* or *interpolation variables* s_x, s_y to practically arbitrary input data x and/or y. Figure 4a shows the use of dither for coarse-quantization estimation of $E\{x\}$. The dither input s_x must

a. Satisfy the condition (15) (for the given class-interval size Δx) to a sufficiently good approximation.
b. Be statistically independent of x.
c. Have zero mean so as not to bias our estimate, *i.e.*, $E\{x+s_x\} = E\{x\}$.
d. Contain no spectral components lower in frequency than the most significant signal components; dither frequencies as high as our apparatus will handle will favor our filtering operations.

Speaking in terms of voltage measurements, $s_x = s_x(t)$ can be a noise voltage or an independent periodic voltage added to the data input $x(t)$. In the latter case,

e. Periodic-dither frequencies must be either incommensurable with the sampling frequency, or they may be cleverly synchronized with the sampling rate so as to generate a "typical" pseudo-random sample of dither over the averaging period (Figure 4c).[22,24]

To approximate the condition (15), s_x must range at least between $-\Delta x/2$ and $\Delta x/2$. The approximation will, generally speaking, improve with larger dither voltages, but the mean-square dither also increases estimate variances (section 7). Triangle-wave or sawtooth dither, which is uniformly distributed over its amplitude range, is convenient. For a peak-to-peak triangle or sawtooth amplitude equal to one class-interval width Δx, it is shown in section 13 that

$$E\{(x+s_x)_Q\} = E\{x\} \tag{16}$$

holds *exactly,* even though the triangle wave satisfies the quantizing theorem only approximately. We can interpret the effect of the dither intuitively as a sort of statistical interpolation which distributes $x+s_x$ more evenly over the discrete sample values of $(x+s_x)_Q$.

For correlation, dither voltages s_x and s_y are added to the respective correlator inputs x and y. s_x and s_y must have zero mean and must be mutually uncorrelated and statistically independent of x and y. For triangle waves s_x, s_y with zero mean, peak-to-peak amplitudes Δx, Δy, and different frequencies,

$$E\{(x+s_x)_Q(y+s_y)_Q\} = E\{xy\} \tag{17}$$

(see also section 13).

Figure 4b illustrates the special case of *one-bit correlation with dither.* For signals x, y both ranging between $-a$ and a, one-bit quantization groups data into two class intervals centered at $-a/2$ and $a/2$, and the class-interval width is $\Delta x = \Delta y = a$. This requires a peak-to-peak amplitude $2a$ for triangle-wave dither. Since the new variables $x+s_x$, $y+s_y$ range between $-2a$ and $2a$, their one-bit quantization corresponds to class-interval centers at $-a$ and a, so that

$$\begin{aligned}(x+s_x)_Q &= a\,\mathrm{sgn}\,(x+s_x)\\ (y+s_y)_Q &= a\,\mathrm{sgn}\,(y+s_y)\end{aligned} \tag{18}$$

The analysis outlined in section 13 shows that

$$E\{\mathrm{sgn}\,(x+s_x)\,\mathrm{sgn}\,(y+s_y)\} = \frac{1}{a^2}E\{xy\} \tag{19}$$

Although the addition of appropriate zero-mean dither will not *bias* our estimates, it can affect estimate *variances.* To minimize variance increases due to dither, we favor the use of periodic dither and

a. Employ as high dither frequencies as practical.
b. Compute finite-time averages over an integral number of dither periods (this implies the use of harmonically related dither frequencies in correlators).
c. Generate "representative" dither samples in the manner of Figure 4c.

7. Effect of Quantization on Statistical Fluctuations. When quantized samples of $x_Q(t)$ are used to compute sampled-data estimates of $E\{x(t_1)\}$, *viz.*,

$$x_Q(t_1) = \frac{1}{n}\sum_{k=1}^{n} {}^k x_Q(t_1) \qquad (20a)$$

(sample average over n independent experiments) or

$$[x_Q]_n = \frac{1}{n}\sum_{k=1}^{n} x_Q(k\Delta t) \qquad (20b)$$

(sampled-data time average for a stationary process), the estimate variances are given by[2]

$$\mathrm{Var}\{\overline{x_Q(t_1)}\} = \frac{1}{n}\mathrm{Var}\{x_Q(t_1)\}$$

$$\mathrm{Var}\{[x_Q]_n\} = \frac{1}{n}\mathrm{Var}\{x_Q\} + \frac{2}{n}\sum_{k=1}^{n-1}\left(1-\frac{k}{n}\right) \qquad (21)$$
$$\{R_{x_Q x_Q}(k\Delta t) - [E\langle x_Q\rangle]^2\}$$

Equations (6) to (10), Table 1, and Figure 2 indicate that these variances will not differ too badly from the corresponding expressions for unquantized data as long as the quantizing theorems hold approximately. In particular, we have in this case

$$\mathrm{Var}\{\overline{x_Q}\} = \frac{1}{n}\mathrm{Var}\{x_Q\} \approx \mathrm{Var}\{\bar{x}\} + \frac{1}{12}\frac{(\Delta x)^2}{n} \qquad (22)$$

Similarly, correlation-estimate variances[2] are not seriously increased by quantization if appropriate second-order and fourth-order joint distributions of the correlator inputs x, y are "band-limited."

If we employ dither (section 6) for coarse-quantization measurements of $E\{x\}$, the dither variance Var $\{s_x\}$ will, approximately,* simply add to the quantization-noise variance $(\Delta x)^2/12$. For triangle-wave dither s_x of peak-to-peak amplitude Δx, $\mathrm{Var}\{s_x\} = (\Delta x)^2/12$, and

$$\mathrm{Var}\{(x+s_x)_Q\} \leq \mathrm{Var}\{x\} + \frac{1}{6}(\Delta x)^2 \qquad (23)$$

For *one-bit correlation* without dither (section 5), we cannot usually apply the quantizing theorem, but we know that the square of the digital multiplier output $\mathrm{sgn}\, x\ \mathrm{sgn}\, y$ in Figure 3a is necessarily always 1. Hence

$$\begin{aligned}\mathrm{Var}\{\mathrm{sgn}\, x\ \mathrm{sgn}\, y\} &= E\{[\mathrm{sgn}\, x\ \mathrm{sgn}\, y]^2\} \\ &\quad - [E\{\mathrm{sgn}\, x\ \mathrm{sgn}\, y\}]^2 \\ &= 1 - [E\{\mathrm{sgn}\, x\ \mathrm{sgn}\, y\}]^2\end{aligned} \qquad (24)$$

where we can substitute the expression (11), when x and y are Gaussian signals with zero mean.

*The exact variance can be computed from equation (35) with the aid of the relation (4).

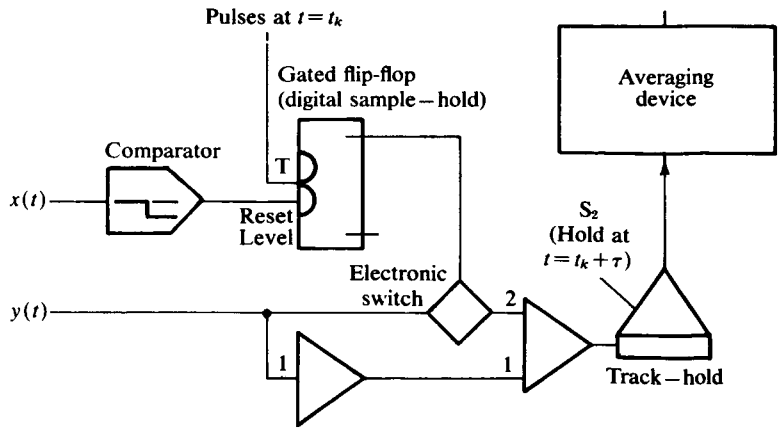

Figure 3b – Approximate correlation employing one-bit quantization of x.

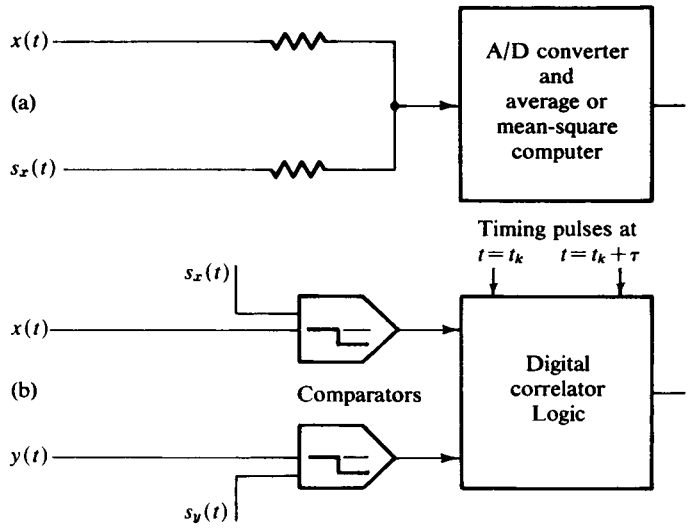

Figure 4a, b – Hybrid analog-digital averaging circuit with dither (a), and one-bit correlator with dither (b).

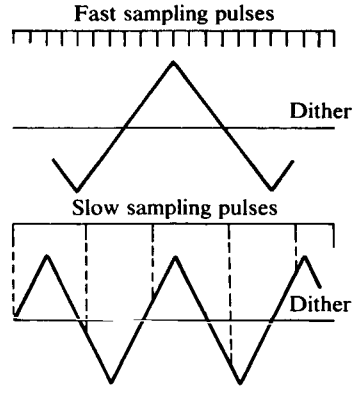

Figure 4c – Synchronization of periodic dither and sampling pulse for fast sampling (approximating continuous averaging) and for slow sampling. The averaging period should equal a (large) integral number of dither periods. Sawtooth waves and staircase waveforms derived from digital counters can replace the triangle-wave dither.

If we have no *a priori* knowledge about x and y other than their range $-a$ to a, one-bit correlation will require dither, say triangle-wave dither with peak-to-peak amplitude $2a$ (section 6). The square of the digital-multiplier output is always 1; recalling equation (16), we find

$$E\{[(x+s_x)_Q(y+s_y)_Q]^2\} = a^4 E\{\operatorname{sgn}(x+s_x)\ \operatorname{sgn}(y+s_y)\} = a^4$$

It follows that

$$\operatorname{Var}\{(x+s_x)_Q(y+s_y)_Q\} = a^4 - [E\{xy\}]^2 \qquad (25)$$

if these quantities exist, no matter how large or small Var $\{xy\}$ is. The possibly very high variance (25) expresses the information loss in one-bit correlation and is the price of equipment simplicity. The resulting estimate variances might turn out to be impractically large for reasonable sample sizes or observation times. In particular, for the independent-sample estimate $\overline{a^2 \operatorname{sgn}(x+s_x)\ \operatorname{sgn}(y+s_y)}$, we find

$$\operatorname{Var}\{\overline{a^2 \operatorname{sgn}(x+s_x)\ \operatorname{sgn}(y+s_y)}\} = \frac{a^4 - [E\{xy\}]^2}{n} \qquad (26)$$

Smit,[26] on the other hand, studied the polarity-coincidence estimates $\overline{\operatorname{sgn} x(t)\ \operatorname{sgn} x(t+\tau)}$ and $\sin\left[\frac{\pi}{2}\overline{\operatorname{sgn} x(t)\ \operatorname{sgn} x(t+\tau)}\right]$ *for the normalized autocorrelation* function $E\{x(t)x(t+\tau)\}/E\{x^2(t)\}$ of Gaussian signals experimentally. Using *closely spaced* (correlated) samples and no dither, he found that the dispersion of the polarity-coincidence estimate was rarely over 150 per cent of the dispersion measured for the conventional estimate $\overline{x(t)x(t+\tau)}/\overline{x^2(t)}$; this was readily overcome through an increase in the sample size. The difference between the percentage errors of the polarity-coincidence and conventional estimates was even smaller. Fluctuation errors of polarity-coincidence correlation estimates surely deserve more theoretical and experimental study.

8. Probability Distribution of the Quantized Variable.

Referring back to section 1 and Figure 1, we consider a continuous random input $x=x(t)$ with first-order probability density $p(x)$ at some sampling time $t=t_1$. The corresponding quantizer output

$$x_Q = x + n_Q = i\Delta x \quad \left(i\Delta x - \frac{\Delta x}{2} < x \leq i\Delta x + \frac{\Delta x}{2};\ i=0, \pm 1, \pm 2, \cdots\right) \qquad (27)$$

is a discrete random variable, but we can represent its distribution by a (symbolic) probability density

$$p_Q(x_Q) = \sum_{i=-\infty}^{\infty} \delta(x_Q - i\Delta x) \int_{i\Delta x - \frac{\Delta x}{2}}^{i\Delta x + \frac{\Delta x}{2}} p(x)\,dx \qquad (28)$$

i.e., by "comb" of impulse functions concentrating the probabilities

$\operatorname{Prob}\left[i\Delta x - \frac{\Delta x}{2} < x \leq i\Delta x + \frac{\Delta x}{2}\right]$ at the class-interval centers $i\Delta x$ (Figure 5a). We rewrite the expression (28) as

$$p_Q(x_Q) = \sum_{i=-\infty}^{\infty} c_i \delta(x_Q - i\Delta x) \qquad (29a)$$

with

$$c_i = \int_{i\Delta x - \frac{\Delta x}{2}}^{i\Delta x + \frac{\Delta x}{2}} p(x)\,dx = \int_{-\infty}^{\infty} p(\lambda - i\Delta x)\ \operatorname{rect}\frac{\lambda}{\Delta x}\ d\lambda \quad (i=0, \pm 1, \pm 2, \cdots) \qquad (29b)$$

where each coefficient appears as a convolution of $p(x)$ and the "rectangle function"

$$\operatorname{rect}\frac{x}{\Delta x} = \begin{cases} 1 & \left(|x| < \frac{\Delta x}{2}\right) \\ 0 & \left(|x| > \frac{\Delta x}{2}\right) \end{cases} \qquad (30)$$

Similarly, for a pair of random variables x,y with joint probability density $p(x,y)$, we can represent the joint distribution of the quantizer outputs x_Q, y_Q by the symbolic density

$$p_Q(x_Q, y_Q) = \sum_{i=-\infty}^{\infty} \sum_{k=-\infty}^{\infty} c_{ik} \delta(x_Q - i\Delta x)\delta(y_Q - k\Delta y) \qquad (31a)$$

with

$$c_{ik} = \int_{-\infty}^{\infty}\int_{-\infty}^{\infty} p(x - i\Delta x, y - k\Delta y)\ \operatorname{rect}\frac{x}{\Delta x}\ \operatorname{rect}\frac{y}{\Delta y}\,dx\,dy \quad (i, k = 0, \pm 1, \pm 2, \cdots) \qquad (31b)$$

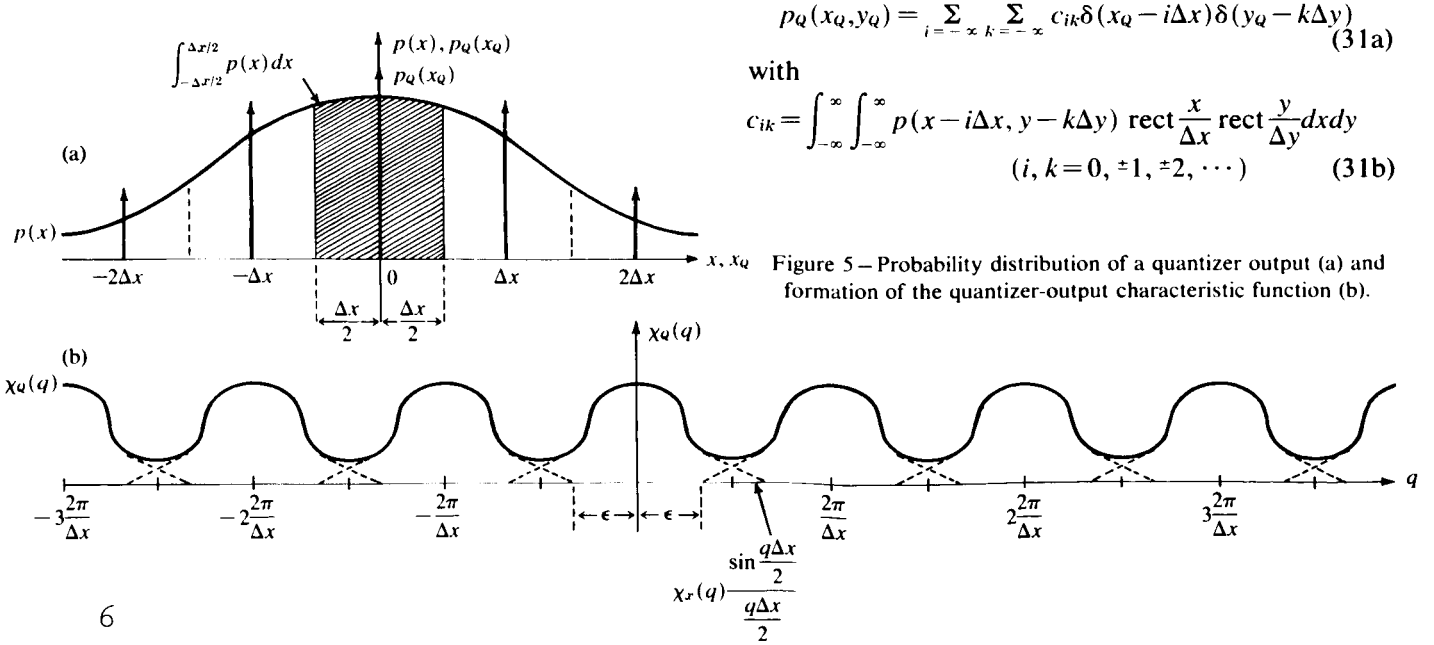

Figure 5 – Probability distribution of a quantizer output (a) and formation of the quantizer-output characteristic function (b).

9. Proof of the Quantizing Theorems.

We recall

$$\int_{-\infty}^{\infty} e^{jqx}\delta(x-i\Delta x)\,dx = e^{jiq\Delta x}$$

to find the characteristic function (section 2) of the quantizer output x_Q, *viz.*,

$$\begin{aligned}\chi_Q(q) &= \int_{-\infty}^{\infty} e^{jqx_Q}\,p_Q(x_Q)\,dx_Q \\ &= \int_{-\infty}^{\infty} e^{jqx_Q}\sum_{i=-\infty}^{\infty} c_i\delta(x_Q-i\Delta x)\,dx_Q \\ &= \sum_{i=-\infty}^{\infty} c_i e^{jiq\Delta x}\end{aligned} \tag{32}$$

This is a Fourier series representing a periodic function with period $2\pi/\Delta x$. Since $2\pi p(\lambda - i\Delta x)$ is the Fourier transform of $e^{-jiq\Delta x}\chi(q)$, and $2\pi\,\mathrm{rect}\,\lambda/\Delta x$ is the Fourier transform of $\Delta x \sin(q\Delta x/2)/(q\Delta x/2)$, we can use Borel's convolution theorem[3] to transform the convolution integrals (29b) into products, so that

$$\begin{aligned}\chi_Q(q) &= \frac{\Delta x}{2\pi}\sum_{i=-\infty}^{\infty} e^{jiq\Delta x}\int_{-\infty}^{\infty} e^{-ji\mu\Delta x}\chi_x(\mu)\,\frac{\sin\frac{\mu\Delta x}{2}}{\frac{\mu\Delta x}{2}}\,d\mu \\ &= \frac{\Delta x}{2\pi}\int_{-\infty}^{\infty}\sum_{i=-\infty}^{\infty} e^{ji\Delta x(q-\mu)}\chi_x(\mu)\,\frac{\sin\frac{\mu\Delta x}{2}}{\frac{\mu\Delta x}{2}}\,d\mu\end{aligned} \tag{33}$$

with suitable convergence implied by the integrability of $p(x)$.[2] Under the integral sign it is safe to employ the symbolic Fourier-series relation

$$\frac{\Delta x}{2\pi}\sum_{i=-\infty}^{\infty} e^{jiq\Delta x} = \sum_{k=-\infty}^{\infty}\delta\left(q-k\frac{2\pi}{\Delta x}\right) \tag{34}$$

It follows that our Fourier series (32) or (33) represents the periodic function

$$\chi_Q(q) = \sum_{i=-\infty}^{\infty}\chi_x\left(q-i\frac{2\pi}{\Delta x}\right)\frac{\sin\left(q-i\frac{2\pi}{\Delta x}\right)\frac{\Delta x}{2}}{\left(q-i\frac{2\pi}{\Delta x}\right)\frac{\Delta x}{2}} \tag{35}$$

obtained through superposition of similar terms displaced by successive multiples of $2\pi/\Delta x$.

If now $\chi_x(q)=0$ for $|q| \geq \frac{2\pi}{\Delta x} - \epsilon$ $(\epsilon>0)$, then adjacent replicas of $\chi_x(q)$ $\sin(q\Delta x/2)(q\Delta x/2)$ in Figure 5b do not overlap in the interval $-\epsilon < q < \epsilon$, *so that*

$$\chi_Q(q) = \chi_x(q)\,\frac{\sin\frac{q\Delta x}{2}}{\frac{q\Delta x}{2}} \quad (|q|<\epsilon) \tag{36}$$

Differentiation of equation (36) relates every existing derivative of $\chi_x(q)$ at $q=0$ uniquely to derivatives of $\chi_Q(q)$ at $q=0$. Remembering equation (4), *we can recover every existing expected value (moment)* $E\{x^m\}$ $m=1,2,\cdots$) *from the quantizer-output distribution if the first-order probability distribution of the input x is "band-limited" so that* $\chi_x(q)=0$ *for* $|q| \geq \frac{2\pi}{\Delta x} - \epsilon(\epsilon>0)$. More specifically, differentiation of equation (36) at $q=0$ yields the important relations (6).

For $\epsilon \geq \pi/\Delta x$, there is no overlap at all in Figure 5b, and $\chi_Q(q)$ defines $\chi_x(q)$ uniquely: *the first-order probability distribution of the input x is completely determined by that of the quantizer output* x_Q *if* $\chi_x(q)=0$ *for* $|q| \geq \pi/\Delta x$. This theorem is similar to (but not identical with) the well-known sampling theorem[3] for band-limited time functions.

Precisely analogous reasoning produces similar results for the joint distributions of two random variables x, y and of two corresponding quantizer outputs x_Q, y_Q. If $\chi_{x,y}(q_1,q_2)=0$ for $|q_1| \geq 2\pi/\Delta x - \epsilon$, $|q_2| \geq 2\pi/\Delta y - \epsilon$ $(\epsilon>0)$, then

$$\chi_Q(q_1,q_2) = \chi_{x,y}(q_1,q_2)\,\frac{\sin\frac{q_1\Delta x}{2}}{\frac{q_1\Delta x}{2}}\,\frac{\sin\frac{q_2\Delta y}{2}}{\frac{q_2\Delta y}{2}} \quad (|q_1|,|q_2|<\epsilon) \tag{37}$$

Differentiation at $q_1=q_2=0$ yields equation (8) and similar relations for higher-order moments. Finally, $\chi_{x,y}(q_1,q_2)$ and hence the joint second-order distribution of x and y is completely determined by that of x_Q and y_Q if $\chi_{x,y}(q_1,q_2)=0$ for $|q_1| \geq \pi/\Delta x, |q_2| \geq \pi/\Delta y$.

10. Properties of Quantization Noise.

If x is in the i^{th} class interval, the first-order probability density of the quantization noise $n_Q = x_Q - x$ is $p_x(n_Q - i\Delta x)\,\mathrm{rect}\,n_Q/\Delta x$. Thus,

$$p_{n_Q}(n_Q) = \sum_{i=-\infty}^{\infty} p_x(n_Q - i\Delta x)\,\mathrm{rect}\frac{n_Q}{\Delta x} \tag{38}$$

The characteristic function $\chi_{n_Q}(q)$ is $1/2\pi$ times the inverse Fourier transform of $p_{n_Q}(n_Q)$. We recall that $2\pi p_x(n_Q - i\Delta x)$ is the Fourier transform of $e^{-jiq\Delta x}\chi_x(q)$, and that $2\pi\,\mathrm{rect}\,n_Q/\Delta x$ is the Fourier transform of $\Delta x \sin(q\Delta x/2)/(q\Delta x/2)$. We again apply Borel's convolution theorem, this time to make transform products into convolutions:

$$\begin{aligned}\chi_{n_Q}(q) &= \frac{\Delta x}{2\pi}\sum_{i=-\infty}^{\infty}\int_{-\infty}^{\infty} e^{-ji\lambda\Delta x}\chi_x(\lambda)\,\frac{\sin(q-\lambda)\frac{\Delta x}{2}}{(q-\lambda)\frac{\Delta x}{2}}\,d\lambda \\ &= \frac{\Delta x}{2\pi}\int_{-\infty}^{\infty}\sum_{i=-\infty}^{\infty} e^{-ji\lambda\Delta x}\chi_x(\lambda)\,\frac{\sin(q-\lambda)\frac{\Delta x}{2}}{(q-\lambda)\frac{\Delta x}{2}}\,d\lambda\end{aligned}$$

We once again employ the relation (34) and find

$$\chi_{n_Q}(q)=\sum_{k=-\infty}^{\infty}\chi_x\left(k\frac{2\pi}{\Delta x}\right)\frac{\sin\left(q-k\frac{2\pi}{\Delta x}\right)\frac{\Delta x}{2}}{\left(q-k\frac{2\pi}{\Delta x}\right)\frac{\Delta x}{2}} \tag{39}$$

If the distribution of our input signal x is "band-limited" so that

$$\chi_x(q)=0 \text{ for } |q|\geq 2\pi/\Delta x, \text{ then}$$

$$\left.\begin{aligned}\chi_{n_Q}(q)&=\frac{\sin\frac{q\Delta x}{2}}{\frac{q\Delta x}{2}} \qquad p_{n_Q}(n_Q)=\frac{1}{\Delta x}\operatorname{rect}\frac{n_Q}{\Delta x}\\ E\{n_Q\}&=0 \qquad \operatorname{Var}\{n_Q\}=E\{n_Q^2\}=\frac{1}{12}(\Delta x)^2\end{aligned}\right\} \tag{40}$$

i.e., the quantization noise is uniformly distributed between $-\Delta x/2$ and $\Delta x/2$.

Precisely analogous reasoning yields the joint distribution of quantization-noise samples $n_{Qx}=x_Q-x$, $n_{Qy}=y_Q-y$. We find

$$\chi_{n_{Qx},n_{Qy}}(q_1,q_2)=\sum_{i=-\infty}^{\infty}\sum_{k=-\infty}^{\infty}\chi_{x,y}\left(i\frac{2\pi}{\Delta x},k\frac{2\pi}{\Delta x}\right)\frac{\sin\left(q_1-i\frac{2\pi}{\Delta x}\right)\frac{\Delta x}{2}}{\left(q_1-i\frac{2\pi}{\Delta x}\right)\frac{\Delta x}{2}}\cdot\frac{\sin\left(q_2-k\frac{2\pi}{\Delta y}\right)\frac{\Delta y}{2}}{\left(q_2-k\frac{2\pi}{\Delta y}\right)\frac{\Delta y}{2}} \tag{41}$$

If $\chi_{x,y}(q_1,q_2)=0$ for $|q_1|\geq 2\pi/\Delta x$, $|q_2|\geq 2\pi/\Delta y$, then

$$\left.\begin{aligned}\chi_{n_{Qx},n_{Qy}}(q_1,q_2)&=\frac{\sin\frac{q_1\Delta x}{2}}{\frac{q_1\Delta x}{2}}\cdot\frac{\sin\frac{q_2\Delta y}{2}}{\frac{q_2\Delta y}{2}}\\ p_{n_{Qx},n_{Qy}}(n_{Qx},n_{Qy})&=\frac{1}{\Delta x\Delta y}\operatorname{rect}\frac{n_{Qx}}{\Delta x}\operatorname{rect}\frac{n_{Qy}}{\Delta y}\\ E\{n_{Qx},n_{Qy}\}&=0\end{aligned}\right\} \tag{42}$$

i.e., the quantization-noise samples *n_{Qx} and n_{Qy} are uniformly distributed and statistically independent,* even though x and y may not be independent.

When the first quantizing theorem of section 3 holds, then equations (6) and (40) imply

$$R_{x,n_Q}(t_1,t_1)=E\{x(t_1)n_Q(t_1)\} \tag{43}$$
$$=\frac{1}{2}[\operatorname{Var}\{x_Q(t_1)\}-\operatorname{Var}\{x(t_1)\}-\operatorname{Var}\{n_Q(t_1)\}]=0$$

It can also be shown[1] that $R_{xn_Q}(t_1,t_2)$ must be zero for all $\tau=t_2-t_1$; hence quantization noise and input are uncorrelated (n_Q is, of course, *not* statistically independent of x, but, indeed, completely determined when x is given). For Gaussian data with $\Delta x<3\sigma$, the expression (43) is not zero, but can be calculated with the aid of Table 1; R_{x,n_Q} is still small.

11. Quantization of Gaussian Variables.[1]

(a) For Gaussian data

$$p(x)=\frac{1}{\sqrt{2\pi\sigma}}e^{-\frac{1}{2}\left(\frac{x-\xi}{\sigma}\right)^2} \qquad \chi_x(q)=e^{-\frac{1}{2}\sigma^2q^2-j\xi q} \tag{44}$$

Substitution of the Gaussian characteristic function $\chi_x(q)$ into equation (35) yields $\chi_Q(q)$. If $\xi=E\{x\}=0$ (Gaussian data with zero mean), then $p_Q(x)$ is, like $p(x)$, an even function, and

$$E\{x_Q^m\}=E\{x^m\}=0 \quad (m=1,3,5,\cdots) \tag{45}$$

In this case $\chi_Q(q)$, too, is an even real function, which looks like Figure 5b; for $\Delta x\leq 3\sigma$, only the terms corresponding to $i=0$, $i=\pm 1$ in equation (35) contribute appreciably to the derivatives of $\chi_Q(q)$ at $q=0$. Specifically, the contribution of the $i=\pm 1$ terms to the derivative at $q=0$ is[1]

$$E\{x_Q^2\}-E\{x^2\}-\frac{1}{12}(\Delta x)^2=-2\sigma^2\left[2+\frac{1}{2\pi^2}\left(\frac{\Delta x}{\sigma}\right)^2\right]e^{-2\pi^2\left(\frac{\sigma}{\Delta x}\right)^2} \tag{46}$$

which was used in the computation of Table 1. Using equation (39), we similarly compute

$$E\{n_Q^2\}-\frac{1}{12}(\Delta x)^2=\frac{(\Delta x)^2}{\pi^2}e^{-2\pi^2\left(\frac{\sigma}{\Delta x}\right)^2} \tag{47}$$

(b) For $\xi=E\{x\}\neq 0$, differentiation of equation (35) yields, in accordance with equation (4),

$$E\{x_Q\}-E\{x\}=\frac{\Delta x}{\pi}e^{-2\pi^2\left(\frac{\sigma}{\Delta x}\right)^2}\sin\frac{2\pi\xi}{\Delta x} \tag{48}$$

if we neglect all terms other than those with $i=0$, $i=\pm 1$. Note that the correction varies sinusoidally with ξ.

(c) For stationary Gaussian data with zero means, the joint distribution of $x_1=x(t_1)$, $x_2(t_2)$ is described by

$$p(x_1,x_2)=\frac{1}{2\pi\sigma^2\sqrt{1-\rho^2}}\exp\left\{-\frac{1}{2\sigma^2(1-\rho^2)}(x_1^2-2\rho x_1x_2+x_2^2)\right\} \tag{49}$$

$$\chi_{x1,x2}(q_1,q_2)=\exp\left\{-\frac{\sigma^2}{2}(q_1^2+2\rho q_1q_2+q_2^2)\right\} \tag{50}$$

where ρ is the correlation coefficient $E\{x_1x_2\}/\sigma^2=R_{xx}(t_2-t_1)/\sigma^2$. Equation (35) yields $\chi_Q(q_1,q_2)$, and differentiation in accordance with equation (4) produces the approximate values of $E\{x_{1Q}x_{2Q}\}$ used in Figure 3.

Note that similar calculations can be carried out for non-Gaussian data as well, as long as the requisite characteristic functions are known and decay reasonably quickly as $|q|$ increases.

12. Shifted Class Intervals, Simplified Correlators, and Unequal Class Intervals.

Watts[17] has extended Widrow's theory to the case of quantization by class intervals shifted with respect to those in Figure 1, *i.e.*,

$$\left.\begin{aligned} a_1 + i\Delta x - \frac{\Delta x}{2} < x \leq a_1 + i\Delta x + \frac{\Delta x}{2}\ (i = 0, \pm 1, \pm 2, \cdots) \\ a_2 + k\Delta y - \frac{\Delta y}{2} < y \leq a_2 + k\Delta y + \frac{\Delta y}{2}\ (k = 0, \pm 1, \pm 2, \cdots) \end{aligned}\right\} \tag{51}$$

(Figure 6). A derivation analogous to that of section 9 yields

$$\chi_Q(q) = \sum_{i=-\infty}^{\infty} e^{2\pi j i \frac{a_1}{\Delta x}} \chi_x\left(q - i\frac{2\pi}{\Delta x}\right) \frac{\sin\left(q - i\frac{2\pi}{\Delta x}\right)\frac{\Delta x}{2}}{\left(q - i\frac{2\pi}{\Delta x}\right)\frac{\Delta x}{2}} \tag{52}$$

$$\chi_Q(q_1, q_2) = \sum_{i=-\infty}^{\infty} \sum_{k=-\infty}^{\infty} e^{2\pi j\left(i\frac{a_1}{\Delta x} + k\frac{a_2}{\Delta y}\right)} \chi_{x,y}\left(q_1 - i\frac{2\pi}{\Delta x}, q_2 - k\frac{2\pi}{\Delta y}\right) \cdot \frac{\sin\left(q_1 - i\frac{2\pi}{\Delta x}\right)\frac{\Delta x}{2}}{\left(q_1 - i\frac{2\pi}{\Delta x}\right)\frac{\Delta x}{2}} \cdot \frac{\sin\left(q_2 - k\frac{2\pi}{\Delta y}\right)\frac{\Delta y}{2}}{\left(q_2 - k\frac{2\pi}{\Delta y}\right)\frac{\Delta y}{2}} \tag{53}$$

These expressions reduce to equations (35) and (37) for $a_1 = a_2 = 0$; the general formulas can be useful where analog-to-digital converters are expressly designed for specific ranges of random variables. A more important application is the one-bit quantization employed in the simplified correlators of section 5. For the one-bit correlator of Figure 3a,

$$a_1 = \frac{\Delta x}{2} = a_2 = \frac{\Delta y}{2} = \frac{a}{2} \tag{54}$$

if both x and y are assumed to range between $-a$ and a, so that equation (53) becomes

$$\chi_Q(q_1, q_2) = \sum_{i=-\infty}^{\infty} \sum_{k=-\infty}^{\infty} (-1)^{i+k} \chi_{x,y}\left(q_1 - \frac{i\pi}{a}, q_2 - \frac{k\pi}{a}\right) \cdot \frac{\sin\left(\frac{a}{2}q_1 - i\pi\right)}{\frac{a}{2}q_1 - i\pi} \cdot \frac{\sin\left(\frac{a}{2}q_2 - k\pi\right)}{\frac{a}{2}q_2 - k\pi} \tag{55}$$

If x alone is quantized, equation (53) is replaced by

$$\chi_Q(q_1, q_2) = \sum_{i=-\infty}^{\infty} e^{2\pi j i \frac{a_1}{\Delta x}} \chi_{x,y}\left(q_1 - i\frac{2\pi}{\Delta x}, q_2\right) \frac{\sin\left(q_1 - i\frac{2\pi}{\Delta x}\right)\frac{\Delta x}{2}}{\left(q_1 - i\frac{2\pi}{\Delta x}\right)\frac{\Delta x}{2}} \tag{56}$$

where we again substitute $a_1 = \Delta x/2$ for one-bit quantization, as in Figure 3b. The results of section 5 follow by differentiation of equations (55) and (56) in accordance with the relation (4).

Further improvements in the quality of coarse-quantization estimates might result from the use of suitably selected *unequal* class intervals. Such techniques, explored in a different context in references 27 to 30, bear further investigation in connection with statistical measurements. Unequal-interval quantization would seem to apply mainly to specialized applications affording a good deal of *a priori* knowledge of signal distributions.

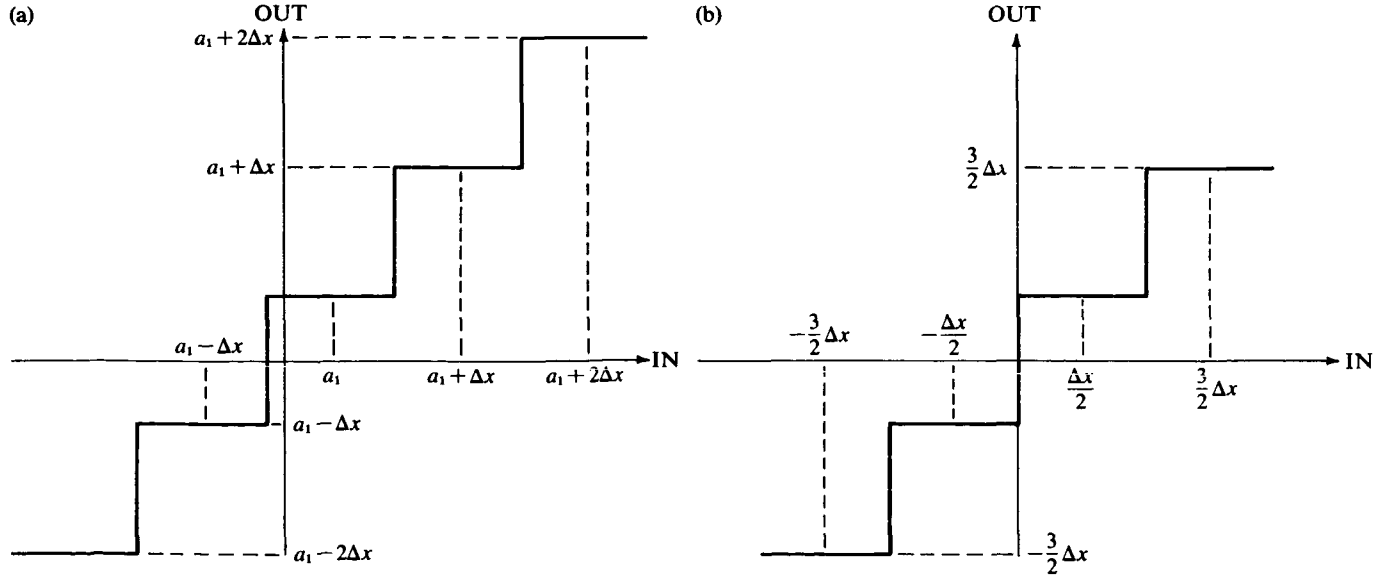

Figure 6 – Quantization with shifted class intervals (a), and the special case $a = \Delta x/2$ (b).

13. Quantization of Signal Plus Dither.

Let x be an input signal which may or may not satisfy a quantizing theorem. We add a dither variable s_x uniformly distributed between $-b$ and b to x (Figure 4a), so that

$$p_{s_x}(s_x)=\begin{cases}\dfrac{1}{2b} & (|s_x|<b)\\ 0 & (|s_x|>b)\end{cases} \qquad \chi_{s_x}(q)=\frac{\sin bq}{bq} \tag{57}$$

Let $s_x=s_x(t)$ be statistically independent of $x(t)$ (random-phase triangle wave whose frequency is not commensurable with that of any periodic component of x). Then, in accordance with equation (14),

$$\chi_{x+s_x}(q)=\chi_x(q)\,\chi_{s_x}(q)=\chi_x(q)\frac{\sin bq}{bq} \tag{58}$$

and equation (52) yields the characteristic function of the quantizer output in Figure 4a

$$\chi_{(x+s_x)_Q}(q)=\sum_{i=-\infty}^{\infty} e^{2\pi j i\frac{a_1}{\Delta x}}\chi_x\left(q-i\frac{2\pi}{\Delta x}\right) \frac{\sin b\left(q-i\frac{2\pi}{\Delta x}\right)}{b\left(q-i\frac{2\pi}{\Delta x}\right)}\frac{\sin\left(q-i\frac{2\pi}{\Delta x}\right)\frac{\Delta x}{2}}{\left(q-i\frac{2\pi}{\Delta x}\right)\frac{\Delta x}{2}} \tag{59}$$

If we choose the dither amplitude b so that

$$b=\frac{\Delta x}{2} \tag{60}$$

then

$$\chi_{(x+s_x)_Q}(q)=\sum_{i=-\infty}^{\infty} e^{2\pi j i\frac{a_1}{\Delta x}}\chi_x\left(q-i\frac{2\pi}{\Delta x}\right)\left[\frac{\sin\left(q-i\frac{2\pi}{\Delta x}\right)\frac{\Delta x}{2}}{\left(q-i\frac{2\pi}{\Delta x}\right)\frac{\Delta x}{2}}\right]^2$$

$$=\sum_{i=-\infty}^{\infty} e^{2\pi j i\frac{a_1}{\Delta x}}\chi_x\left(q-i\frac{2\pi}{\Delta x}\right)\frac{1-\cos(q\Delta x)}{(q\Delta x-2\pi i)^2} \tag{61}$$

For $a_1=0$ or $a_1=\Delta x/2$ (see also section 12), differentiation of equation (61) at $q=0$ in accordance with equation (4) produces the *exact* result

$$E\{(x+s_x)_Q\}=E\{x\} \tag{62}$$

even though the distribution of $x+s_x$ is only approximately "band-limited." Quite similarly, we can add uncorrelated dither samples s_x, s_y (samples of triangle waveforms with different frequencies and amplitudes $\Delta x/2$, $\Delta y/2$) to the input signals x, y of a correlator and find

$$E\{(x+s_x)_Q(y+s_y)_Q\}=E\{xy\} \tag{63}$$

(see also Figure 4b).

ACKNOWLEDGMENTS

The writer would like to express his appreciation to Dr. B. P. Th. Veltman of the Technical University Delft for helpful discussions, and for kindly furnishing copies of references 23 to 26 which are, unfortunately, not widely available.

The writer is grateful to the Air Force Office of Scientific Research and to the National Aeronautics and Space Administration for their joint support of this work.

REFERENCES AND BIBLIOGRAPHY

1 WIDROW B
A Study of Rough Amplitude Quantization by Means of Nyquist Sampling Theory
Trans IRE/PGCT December 1956 see also
Tech Rept 2103-1 Stanford Electronics Laboratories Stanford California 1960

2 DAVENPORT W B W L ROOT
Random Signals and Noise
McGraw Hill NY 1958

3 KORN G A T M KORN
Mathematical Handbook for Scientists and Engineers
McGraw Hill NY 1961

4 KAISER J F R K ANGELL
New Techniques and Equipment for Correlation Computation
Tech Memorandum 7668-TM-2 Servomechanisms Lab Massachusetts Inst of Tech December 1957

5 MAYBACH R
Hybrid Analog-digital Measurement of Sample Averages and Correlation Functions
ACL Memo 85 Electrical Engineering Department University of Arizona 1964

6 MC FADDEN J A
The Correlation Function of a Sine Wave Plus Noise After Extreme Clipping
Trans IRE/PGIT June 1956

7 BECKER C L J V WAIT
Two-level Correlation on an Analog Computer
IRETEC December 1961

8 EKRE H
Polarity-coincidence Correlation Detection of a Weak Noise Source
Trans *IEEE/PGIT* January 1963

9 COOPER R
Crosscorrelation with Binary Signals
Memorandum Electrical Engineering Dept Purdue University 1962

10 ROSENHECK B M
Detecting Signals by Polarity Coincidence
Electronics January 29 1960

11 BUSSGANG J J
Crosscorrelation Functions of Amplitude-Distorted Gaussian Signals
RLE Report No 216 Massachusetts Inst of Tech Cambridge Mass 1952

12 JESPERS P et al
A New Method to Compute Correlation Functions
Intern Symposium on Information Theory Liège Belgium 1962 see *Trans IRE/PGIT* September 1962

13 VAN VLECK J H
The Spectrum of Clipped Noise
Report 51 Radio Research Laboratory Harvard University 1943

14 BENNETT W R
Spectra of Quantized Signals
BSTJ July 1948

15 BOHN E V
A Continuously Acting Adaptive Analog Computer for Determining the Impulse Response of Control Systems with Gaussian Signals
Trans Eng Inst of Canada 5 No 3 1961

16 KOSYAKIN A A
The Statistical Theory of Amplitude Quantization
Automatika i Telemekhanika June 1961

17 WATTS D G
A General Theory of Amplitude Quantization with Applications to Correlation Determination
IEE Monograph No 481 M November 1961

18 BONNET G
Sur La Statistique du Second Ordre des Signaux Aleatoires Quantifies
Comptes Rendus de l'Academie des Sciences 255 825 1962

19 FURMAN G G
Improving the Quantization of Random Signals by Dithering
Report Rand Corp Santa Monica Calif May 1963

20 VELTMAN B P TH H KWAKERNAAK
Theorie und Technik der Polaritatskorrelation für die dynamische Analyse niederfrequenter Signale und Systeme
Regelungstechnik September 1961

21 VELTMAN B P TH A VAN DEN BOS
On the Applicability of the Relay- and Polarity-coincidence Correlator in Automatic Control
Proc IFAC Conference Basel 1963

22 VELTMAN B P TH
Unpublished communication

23 VAN DEN BOS A
Calculation of Correlation Functions by the Polarity-coincidence Method
Research Report Dept of Tech Physics Tech University Delft Netherlands October 1962

24 VAN BEMMEL J H
Calculation and Measurement of Correlation Functions with the Aid of Dither
Research Report Dept of Tech Physics Tech University Delft Netherlands October 1963

25 VAN LOON D
Properties of Quantized Statistical Signals
Research Report Dept of Tech Physics Tech University Delft Netherlands October 1963

26 SMIT H J P
Dispersion of Autocorrelation Estimates
Thesis Dept of Tech Physics Tech University Delft Netherlands 1963

27 MAX J
Quantizing for Minimum Distortion
Trans IRE/PGIT March 1960

28 BRUCE J D
Optimum Quantization for a General Error Criterion
MIT Quarterly Progress Rept No 69 April 1963

29 BLUESTEIN L I R J SCHWARZ
Optimum Zero-memory Filters
Trans IRE/PGIT October 1962

30 BLUESTEIN L I
Asymptotically Optimum Quantizers and Optimum Analog to Digital Converters for Continuous Signals
Trans IEEE/PGIT July 1964

31 MC FADDEN J A
The Fourth Product Moment of Infinitely Clipped Noise
Trans IRE/PGIT December 1958

32 WALLI C R
Quantizing and Sampling Errors in Hybrid Computation
Proc Fall Joint Computer Conf 1964

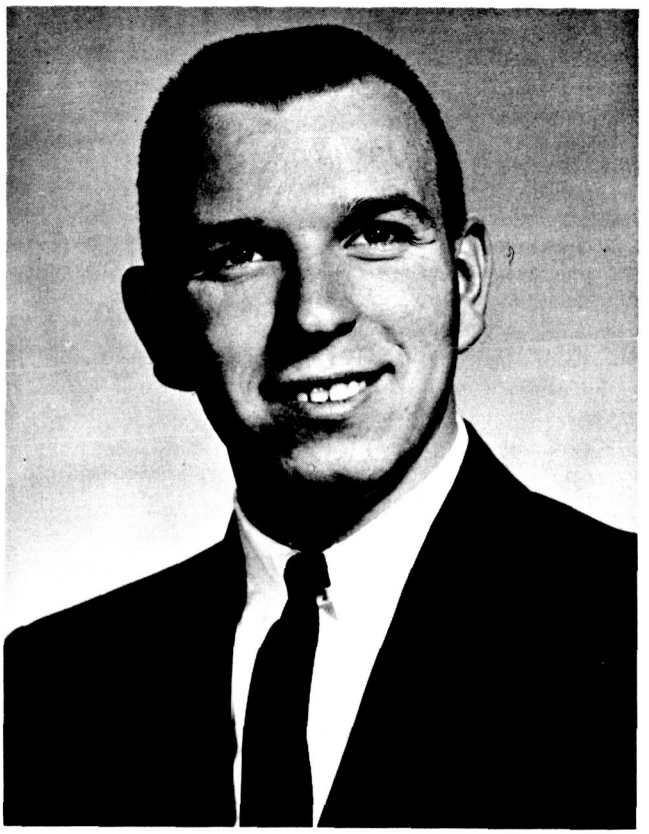

JAMES L. MELSA is at present doing research in the area of sub-optimal control for a Ph.D. dissertation at the University of Arizona, where he has held an appointment as an instructor of electrical engineering since 1961. Previously he was employed by the RCA Surface Communications Laboratory at Vail, Arizona, and did graduate work at the University of Arizona under the RCA Graduate Study Program. Mr. Melsa received his B.S. in electrical engineering from Iowa State University in May 1960 and his MSEE from the University of Arizona in January 1962. He is a member of Tau Beta Pi, Pi Mu Epsilon, Eta Kappa Nu, Phi Kappa Phi, is an associate member of the Society of Sigma Xi, and a student member of the IEEE. His published papers include articles on sampled data control systems and on the electronic simulation of the "biological clock."

MICHAEL J. WOZNY is at present completing requirements toward the Ph.D. degree at the University of Arizona, working in the area of nonlinear and optimal control systems. In 1962-1963 he held a General Electric (Computer Division, Phoenix) Graduate Fellowship at the University. He was an instructor of electrical engineering at the University of Arizona during the 1961-1962 academic year. Mr. Wozny was granted the degrees of BSEE and MSEE by the University of Arizona in 1960 and 1962, respectively, and is a member of Tau Beta Pi and the IEEE. In April 1963 he presented a paper on optimal control at the Southwestern IEEE Conference in Dallas.

EDITOR'S NOTE:

This is definitely not a high-school subject. The specific purpose of this paper is to show that modern iterative analog computation goes well with sophisticated theoretical models.

Iterative-Differential-Analyzer Study of Prediction Networks

by JAMES L. MELSA and MICHAEL J. WOZNY

Department of Electrical Engineering

University of Arizona

ABSTRACT

Iterative-differential-analyzer methods are presented which allow experimental studies of prediction networks to be performed without the use of delay lines. Two classes of problems are examined in this paper:

1. Prediction of stochastic signals with no noise present.

2. Prediction and filtering of deterministic signals masked by noise. Measurement techniques are developed for each case, and experimental verification is included.

INTRODUCTION

The basic problem in experimental studies of prediction networks is that some form of time delay is needed in order to measure the errors involved in a given predictor design. Since accurate delay lines are not readily available, it is desirable to examine other methods of delay.

This paper describes a method of time delay which makes use of the digitally timed track-hold circuits of ASTRAC I,[1] an iterative-differential analyzer. The method given is ideally suited to the study of nonlinear prediction networks. (A block diagram of the ASTRAC I system is shown in Figure 1.)

Prediction networks have been studied on DC analog computers using a power spectral density approach, but this method requires repeated runs, hence a large expenditure of time or equipment.[2]

The Wiener prediction filter design for a stochastic signal with no noise is examined first to demonstrate the repetitive analog technique. The technique is then applied to the examination of the finite-time-finite-order prediction system of Zadeh and Ragazzini. Simple examples were used in this paper so that exact theoretical results could be obtained and compared with the experimental results. The distinct feature of the measurement techniques is that they apply directly to both nonlinear and time-varying systems.

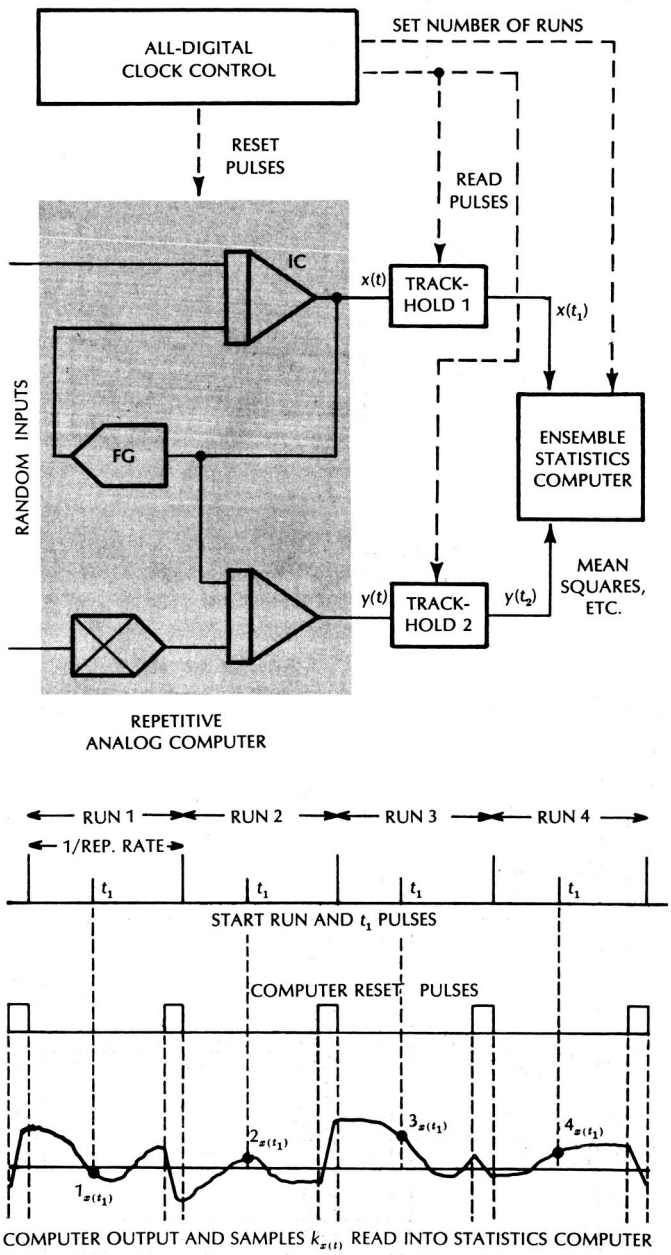

Figure 1 – The ASTRAC I System

PREDICTION OF RANDOM SIGNALS WITH NO NOISE

The characteristics of the linear Wiener prediction filter, optimum in the least-square sense, are considered in detail in this section. The basic equations are presented, and the filter operation examined experimentally on an iterative-differential-analyzer.

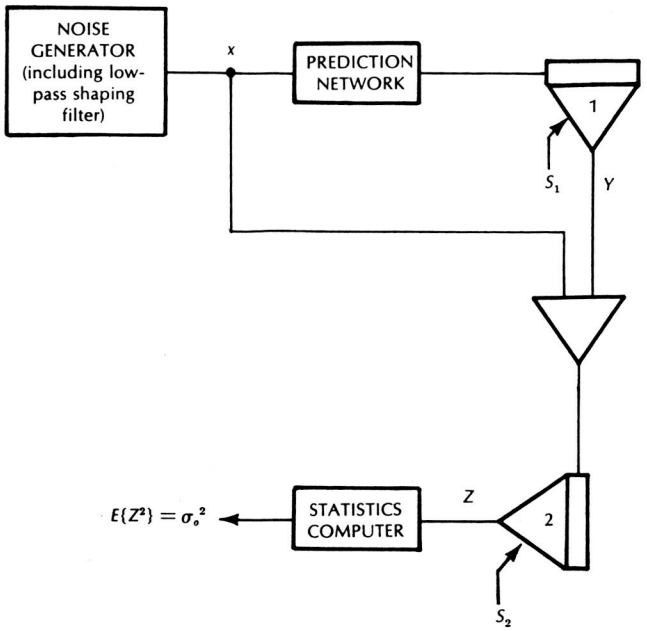

Figure 2 – Computer Diagram for Measuring Mean Square Error of Wiener Prediction Filter Example

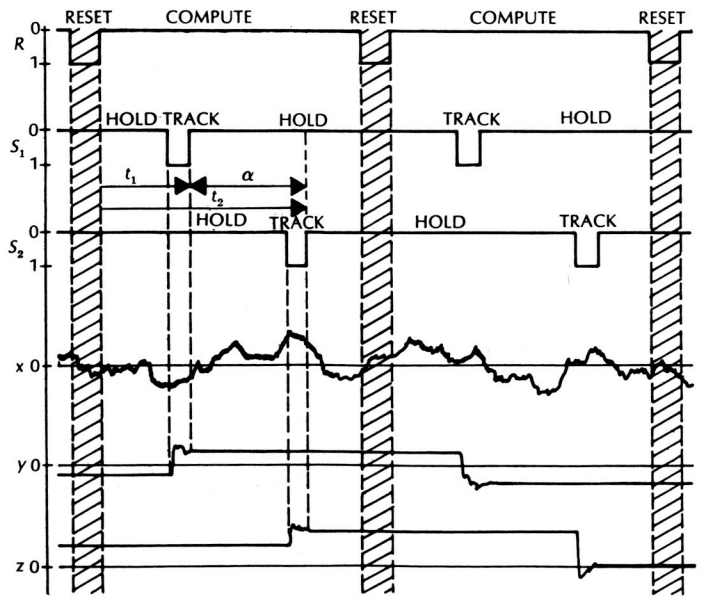

Figure 3 – Timing Diagram for Wiener Filter Example

A. *Design Equations*

A random signal was obtained by passing a random telegraph wave with Poisson distributed event points through a first-order, low-pass filter. The resulting normalized autocorrelation function as defined and derived in reference 3 is

$$R_{ss}(\tau) = e^{-\omega_c|\tau|} \tag{1}$$

where ω_c is the cut-off frequency of the first-order, low-pass shaping filter.

If the desired prediction time is α, the required optimum Wiener prediction filter* is an attenuator

$$H_o = e^{-\omega_c\alpha} \tag{2}$$

The resulting normalized mean square error is then

$$\sigma^2_{opt} = (1 - e^{-2\omega_c\alpha}) \tag{3}$$

B. *Measurement Technique*

The time delay required for making error measurements was obtained by controlling the time interval between the sampling operations of two track-hold circuits. The block diagram of the measuring technique is shown in Figure 2, and the corresponding timing diagram in Figure 3. The mean square value of the output of track-hold circuit 2 was computed using the statistics computer.[4]

C. *Experimental Verification*

Since the primary goal of this study was to evaluate the proposed measurement technique, the entire dynamic range of the digital time control of ASTRAC I was used. For reasons of accuracy this required three separate time delay ranges, each with a different cut-off frequency of the random signal spectral density; see Table 1.

TABLE 1 – *Dynamic Range of Time Delay*

	Shaping filter cutoff frequency, cps			Normalized MSE (calc.)	H_0
	1000	100	10		
Time Delay (ms)	0.1	1	10	0.181	0.905
	0.2	2	20	0.330	0.819
	0.4	4	40	0.550	0.670
	0.7	7	70	0.753	0.497
	1.0	10		0.865	0.368

*The derivation of the Wiener filter appears in many books and therefore will not be given here. See for example Bendat, *Principles and Applications of Random Noise Theory*, p. 179.

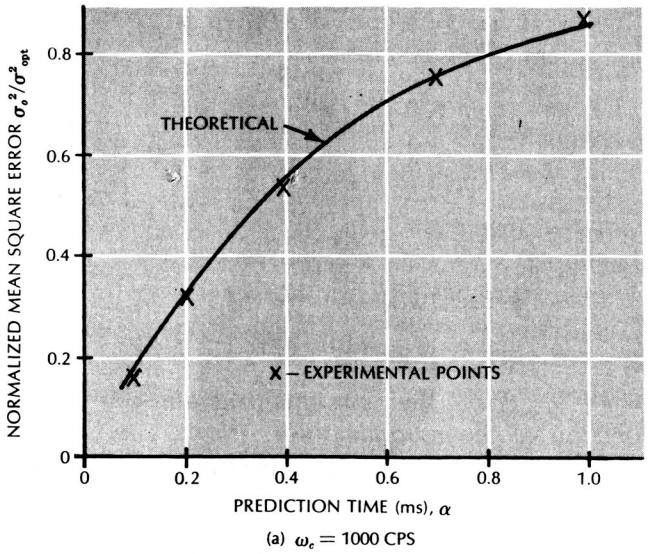

(a) $\omega_c = 1000$ CPS

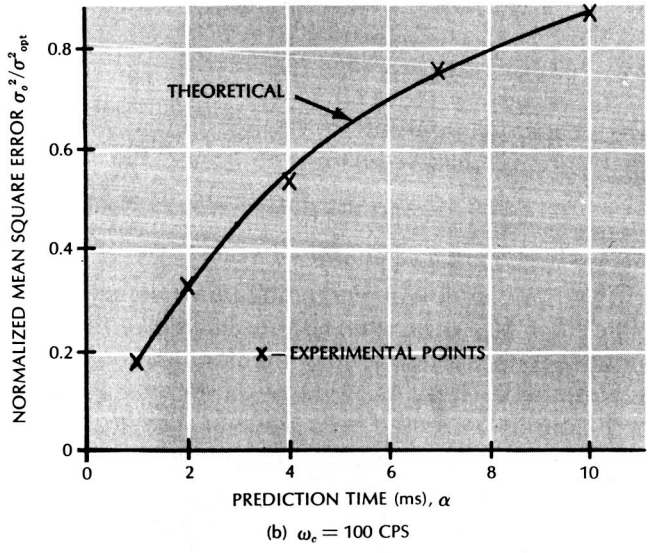

(b) $\omega_c = 100$ CPS

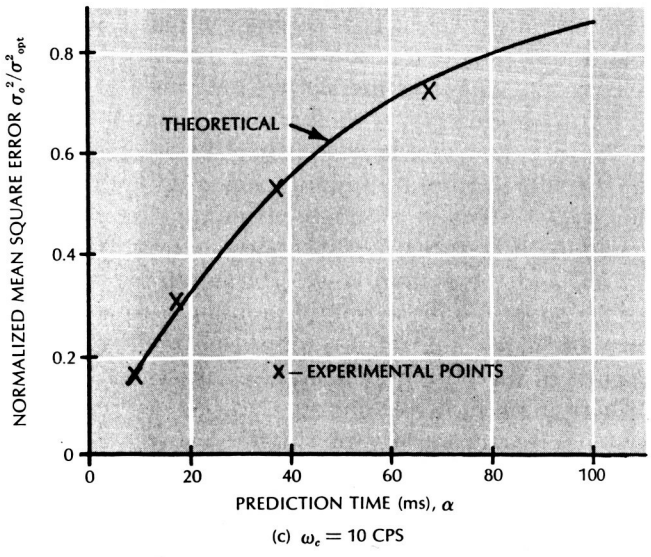

(c) $\omega_c = 10$ CPS

Figure 4 – Normalized Mean Square Error for Various Prediction Times and Cutoff Frequencies

To minimize computer errors the normalized error was used, *i.e.*, the ratio of the mean square error to the mean square value of the input signal. Also the mean square value of the input signal was measured through the track-hold circuit 2 so that any offset would be "calibrated out" in the normalizing of the mean square error.

Data to within 2 per cent of the theoretical values was obtained over the range of prediction times 0.4 ms to 70 ms. The errors for very short time delays, less than 0.4 ms, were approximately in the 10 μsec range of accuracy of the ASTRAC I computer clock. For very long delays the errors became slightly larger than 2 per cent with the measured value being smaller than the calculated value. The curves for the three time ranges studied are given in Figure 4.

The effect of non-optimum prediction networks on mean square error was also studied. The mean square value for a non-optimum filter, $H = \zeta H_o$, was found to be

$$\frac{\sigma_o^2}{\sigma^2_{opt}} = \frac{1 - 2\zeta H_o^2 + \zeta^2 H_o^2}{1 - H_o^2} \tag{4}$$

Plotting $\frac{\sigma_o^2}{\sigma^2_{opt}}$ as a function of ζ provides an indication of the required tolerance in designing the prediction filter. See Figure 5 for an experimental curve.

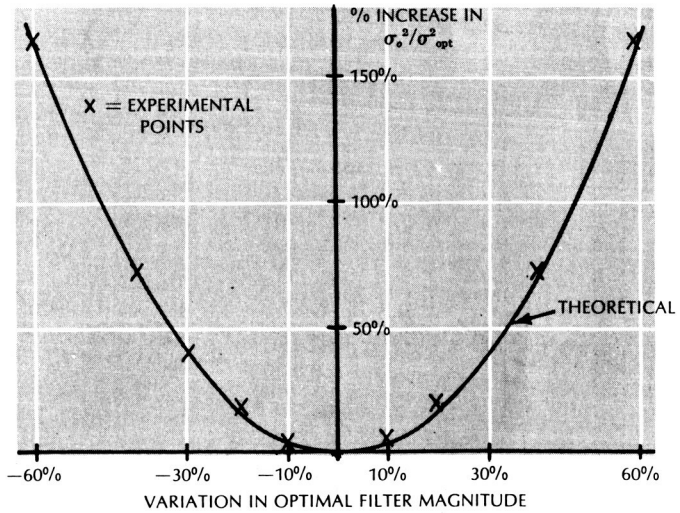

Figure 5 – Effect of Variations in Optimum Filter Magnitude for Prediction Time of 1 ms and a Cutoff Frequency of 100 cps

PREDICTION OF A DETERMINISTIC SIGNAL IN RANDOM NOISE

Although the prediction and filtering of a deterministic signal which is masked by random noise may be handled in a manner similar to that presented in the previous section, another method is presented here to show the power of iterative-differential-analyzer techniques in the study of prediction. The method presented here was first introduced by Zadeh and Ragazzini in 1950[5] and is termed the finite-time-finite-order system. A brief presentation of the design equations is followed by the development of a measurement technique. Finally, an example is presented with experimental verification.

A. *Design Equations*

The finite-time-finite-order system is based on the following design requirements:

1. The system must yield no error after a finite observation time, T, when the noise power is negligible.
2. The mean square value of the output noise is to be minimized.

Consider the system shown in Figure 6. The desired output $v(t)$ is obtained by a given linear, time-invariant operation on $r(t)$. The system input is masked by an additive stationary random noise $n(t)$.

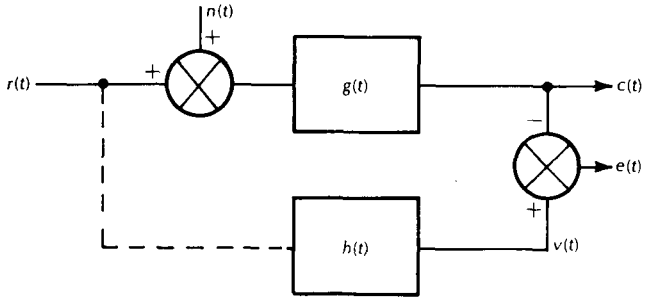

Figure 6 – Finite-Time, Finite-Order System

The input function $r(t)$ is restricted to be a linear combination of known signals $f_i(t)$ with unknown coefficients A_i

$$r(t) = \sum_{i=1}^{M} A_i f_i(t) \tag{5}$$

where the set of known functions satisfies the following equations

$$f_i(t+\tau) = \sum_{j=1}^{M} a_{ij}(\tau) f_j(t). \tag{6}$$

Under these conditions the optimum finite memory system $g_o(t)$ is given by

$$g_o(t) = \sum_{i=1}^{M} \lambda_i g_{oi}(t) \qquad 0 < t < T \tag{7}$$
$$= 0 \text{ otherwise}$$

with $g_{oi}(t)$ given by

$$\int_0^T g_{oi}(t_2)\phi_{nn}(t - t_2)dt_2 = f_i(T - t) \tag{8}$$
$$\text{for } 0 < t < T$$

where $\phi_{nn}(\tau)$ is the unnormalized autocorrelation function of the random noise. The M coefficients, λ_i, are evaluated by substitution of $g_o(t)$ into M constraint equations

$$\int_0^T g_o(t) f_i(T - t)dt = \int_{-\infty}^{\infty} h(t) f_i(T - t)dt$$
$$i = 1, 2, \ldots, M \tag{9}$$

The reader is referred to Chang[6] for a complete derivation of these equations.

B. *Measurement Technique*

The basic problem encountered when trying to experimentally verify the system derived in the previous section is that the finite memory feature necessitates a delay line. An iterative-differential analyzer technique is presented here which makes it possible to measure the mean square value of the output noise without the use of a delay line.

The technique centers about the following argument. Consider a system $g_I(t)$ which has an impulse response identical to $g_o(t)$ during the first T seconds but is not zero thereafter. If the noise is gated into this system at t_o and the output measured at $t_o + T$, it must be identical with the output that the finite memory system would yield; since in both cases only a finite duration of noise input was used. By running the $g_I(t)$ system in a repetitive mode, the noise is gated into the system for T seconds, an output sample taken, and the system reset. The ensemble average of the square of these output samples is equal to the mean square value of the output noise. The equivalence of the ensemble average to the mean square value can be shown in a more rigorous mathematical manner by considering the system shown in Figure 7.

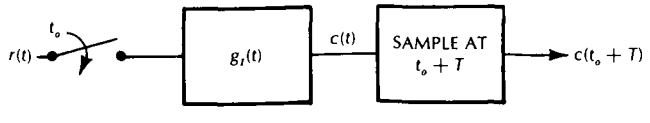

Figure 7 – The $g_I(t)$ System

If the switch is closed at $t=t_o$, and the output sampled at $t=t_o+T$, then:

$$c(t_o+T)=\int_o^\infty g_I(\lambda)n(t_o+T-\lambda)d\lambda$$

But

$$n(t_o+T-\lambda)=0 \quad \text{for} \quad t_o+T-\lambda<t_o \quad \text{and for } \lambda>T.$$

Therefore

$$c(t_o+T)=\int_o^T g_I(\lambda)n(t_o+T-\lambda)d\lambda$$

and

$$E\{c^2(t_o+T)\}=E\left\{\int_o^T\int_o^T g_I(\lambda_1)g_I(\lambda_2)n(t_o+T-\lambda_1)\,n(t_o+T-\lambda_2)d\lambda_1 d\lambda_2\right\} \tag{10}$$

Now interchanging the order of expectation and integration gives

$$E\{c^2(t_o+T)\}=\int_o^T\int_o^T g_I(\lambda_1)g_I(\lambda_2)\phi_{nn}(\lambda_1-\lambda_2)d\lambda_1 d\lambda_2$$

But by definition:

$$g_I(\lambda)=g_o(\lambda) \text{ for } 0<\lambda<T$$

therefore

$$E\{c^2(t_o+T)\}=\int_o^T\int_o^T g_o(\lambda_1)g_o(\lambda_2)\phi_{nn}(\lambda_1-\lambda_2)d\lambda_1 d\lambda_2 \tag{11}$$

which is the mean square value of the output noise for the $g_o(t)$ system. Thus the equivalence is demonstrated.

In general it is possible to build the $g_I(t)$ system without the use of a delay line. This may be done by building the $g_o(t)$ system but not including the delay line portion which gives it a finite memory. Since this $g_I(t)$ will normally become unstable for t much larger than T, it is desirable to reset the system relatively soon after the finite observation time, T.

By the use of the $g_I(t)$ system it is possible to study the transient behavior of the system during the first T seconds after a change in the input has occurred. This may appear to be rather insignificant, but if the system is properly designed the error will be zero after T seconds and the first T seconds will contain all of the transient information.

C. *An Example of Finite-Memory Prediction System*

As a specific case, consider the following problem: A signal $r(t)=a_o+a_1t$ with unknown coefficients a_o and a_1 is masked by white noise, $\phi_{nn}(\tau)=N^2\delta(\tau)$. Determine $g_o(t)$ of a system which gives unerring prediction for α seconds ahead if the noise power is zero and has minimum mean square output noise. Solving for the optimum finite memory system

$$g_o(t)=\frac{1}{T}\left[\left(4+\frac{6\alpha}{T}\right)-\left(6+\frac{12\alpha}{T}\right)\frac{t}{T}\right] 0<t<T$$
$$=0 \text{ otherwise.} \tag{12}$$

Thus the optimum system is independent of N^2, a_o and a_1 as would be expected. Using this system as an example, experimental verification will be made of the measurement technique presented in the previous section.

D. *Experimental Verification of Measurement Technique*

It was decided to use a range of T from 30 to 80 milliseconds and α from 0 to 20 milliseconds. A basic factor leading to this choice was that for smaller values of T the gain of the system was excessive, and for larger values, taking a sufficient number of samples was a prohibitively long process.

The noise source used in the experimental work was a random telegraph wave with Poisson-distributed event points filtered by a first-order, low-pass shaping filter. The unnormalized autocorrelation is

$$\phi_{xx}(\tau)=\frac{M^2\omega_c}{2\beta}e^{-\omega_c|\tau|} \tag{13}$$

Where M is the magnitude of the random telegraph wave, β is the mean count rate and ω_c is the cut-off frequency of the shaping filter. If the bandwidth of the system is much less than ω_c, the ratio of output to input mean square value is

$$\frac{\sigma_{n_o}^2}{\sigma_n^2}=\frac{8}{\omega_c T}\left[1+3\frac{\alpha}{T}+3\left(\frac{\alpha}{T}\right)^2\right] \tag{14}$$

since the input may be assumed to be white noise with mean square value $\frac{M^2\omega_c}{2\beta}$.

Unfortunately due to the finite memory nature of the system, it was rather difficult to get a meaningful measure of bandwidth. An alternate path was to find the actual ratio of output to input mean square value assuming that the input noise had the correlation function of Equation (13) rather than being white noise.

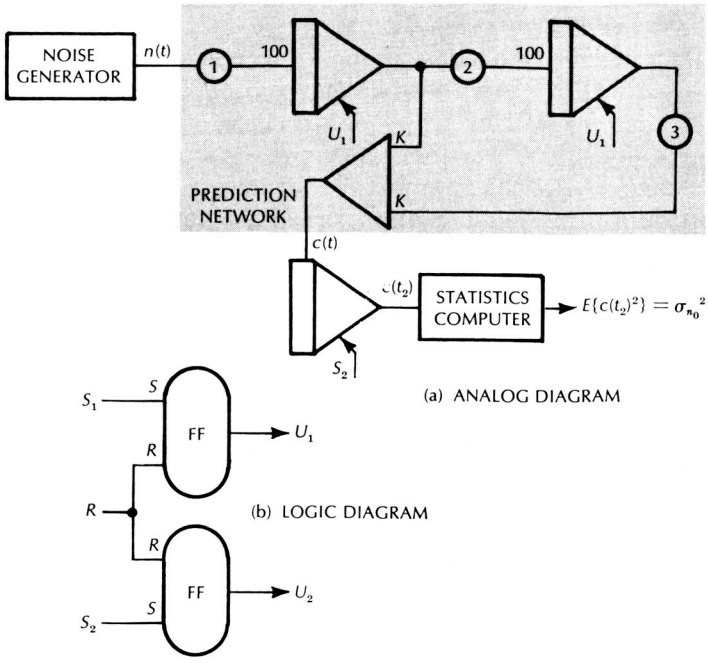

Figure 8 – Computer Diagram for Measuring Mean Square Output Noise for the Finite-Time, Finite Order Example

The resulting ratio of mean square output to mean square input is:

$$\frac{\sigma_{n_o}^2}{\sigma_n^2} = \frac{8}{\omega_c T}\left[1+3\frac{\alpha}{T}+3\left(\frac{\alpha}{T}\right)^2\right]-\left(\frac{2}{\omega_c T}\right)^2$$

$$\times\left[5+18\left(\frac{\alpha}{T}\right)+18\left(\frac{\alpha}{T}\right)^2\right]-\frac{72}{(\omega_c T)^3}\left[1+4\frac{\alpha}{T}+4\left(\frac{\alpha}{T}\right)^2\right] \quad (15)$$

The first term can be recognized as that resulting from the white noise assumption. The last two terms are the corrections due to the fact that the input was actually a filtered random telegraph wave. These correction terms become appreciable at the smallest values of T and larger values of α. The experiment as set up on an iterative-differential-analyzer is shown in Figure 8; a timing diagram is shown in Figure 9.

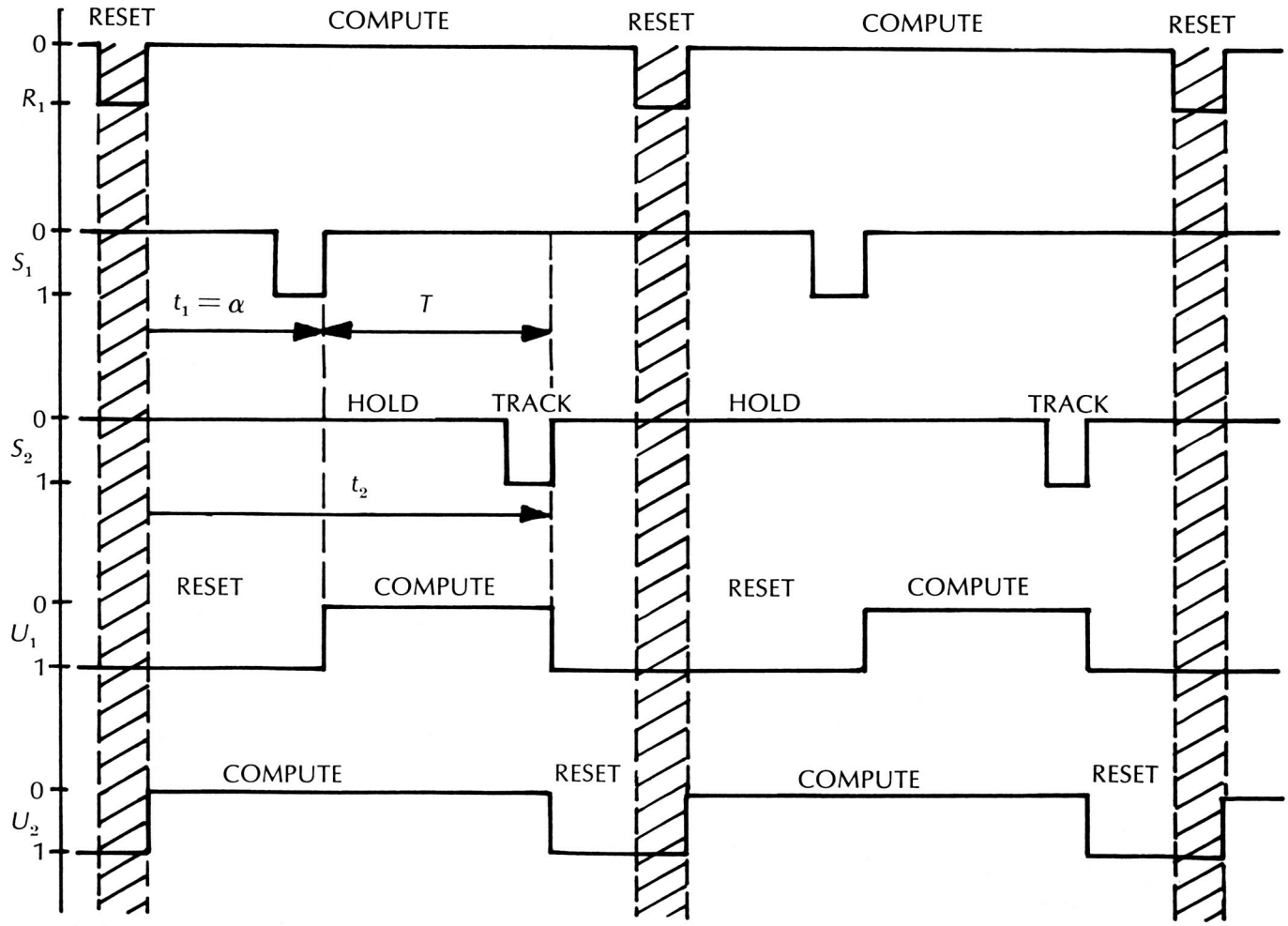

Figure 9 – Timing Diagram for Finite-Time, Finite Order Example

The values of the potentiometers 1, 2, and 3, and the gain K are given in Table 2 for various values of T and α.

TABLE 2 – *Potentiometer Settings and Amplifier Gain*

T_{ms}	α_{ms}	Pot. 1	Pot. 2	Pot. 3	K
30	10	1.00	1.00	.555	2
40	10	.694	.696	.583	2
50	10	.520	.624	.518	2
60	10	.416	.462	.580	2
70	10	.347	.429	.529	2
80	10	.297	.223	.890	2
50	0	.800	.508	.593	1
50	5	.920	.532	.450	1
50	20	.640	.540	.631	2

Using this experimental facility, the ratio of mean square output to mean square input was determined experimentally. These experimental points are plotted on Figures 10 and 11 and show very good correspondence with the theoretical values given by Equation (15).

The transient behavior of the system to the input signal $r(t)$ was also studied. It was decided to determine experimentally the integral square error for a ramp input, $r(t) = Bt$ with various values of observation and prediction time. The theoretical value of normalized ISE was found to be

$$\frac{\text{ISE}}{B^2} = \frac{1}{T^3}\left[\frac{1}{105} + \frac{11\left(\frac{\alpha}{T}\right)}{105} + \frac{13\left(\frac{\alpha}{T}\right)^2\left(\frac{\alpha}{T}\right)^3}{35} + \frac{}{3}\right] \tag{17}$$

In order to make the experimental measurements, it was necessary to modify slightly the system shown in Figure 10. The experimental set-up used is shown in Figure 12. The noise generator has been replaced by two two-mode integrators which were used to generate $r(t)$ and $r(t+\alpha)$. The values of potentiometers 1, 2, 3, and gain K are given in Table 2; the

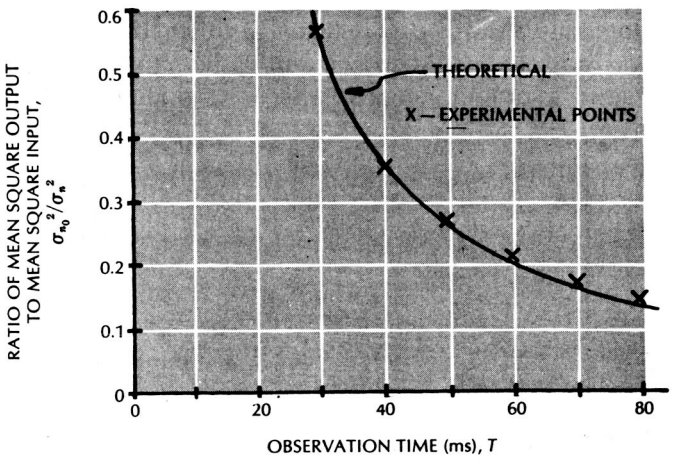

Figure 10 – Variation of Mean Square Output as a Function of Observation Time with Constant Prediction Time of 10 ms

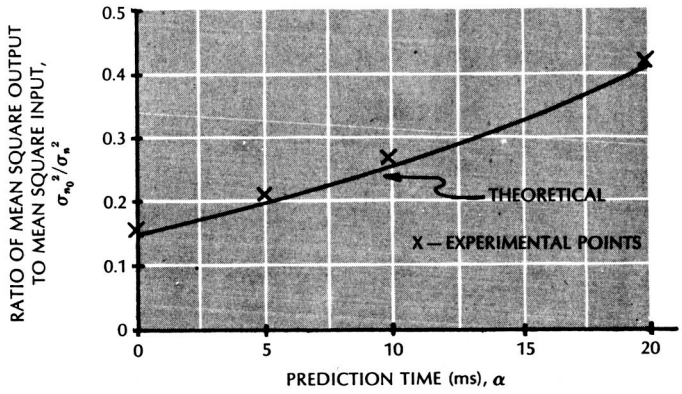

Figure 11 – Variation of Mean Square Output to Mean Square Input as a Function of Prediction Time for Constant Observation Time of 50 ms

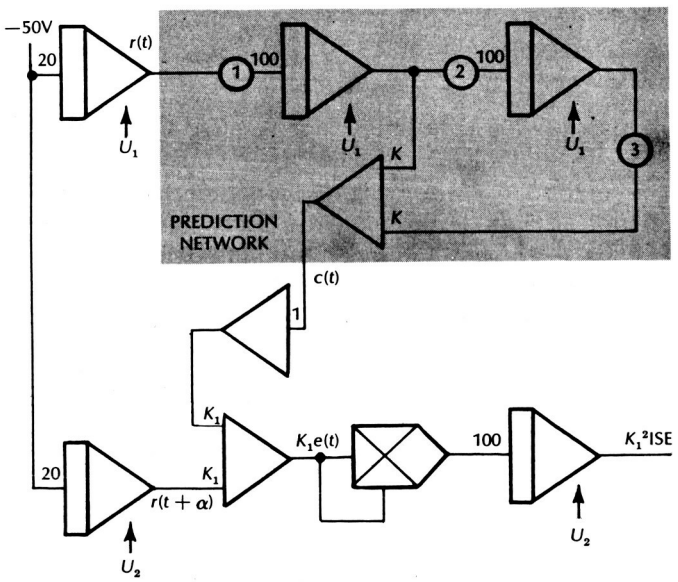

(NOTE: See Figures 8 and 9 for logic and timing diagrams.)

Figure 12 – Computer Diagram for Measuring Integral Square Error for Finite-Time, Finite Order Example

nominal value of B was taken as 1000. The gain K_1 was adjusted to keep the multiplier input voltage within a proper range for accurate operation. The theoretical and experimental values of ISE/B^2 for various T and α are plotted in Figures 13 and 14. Again good correspondence is noted.

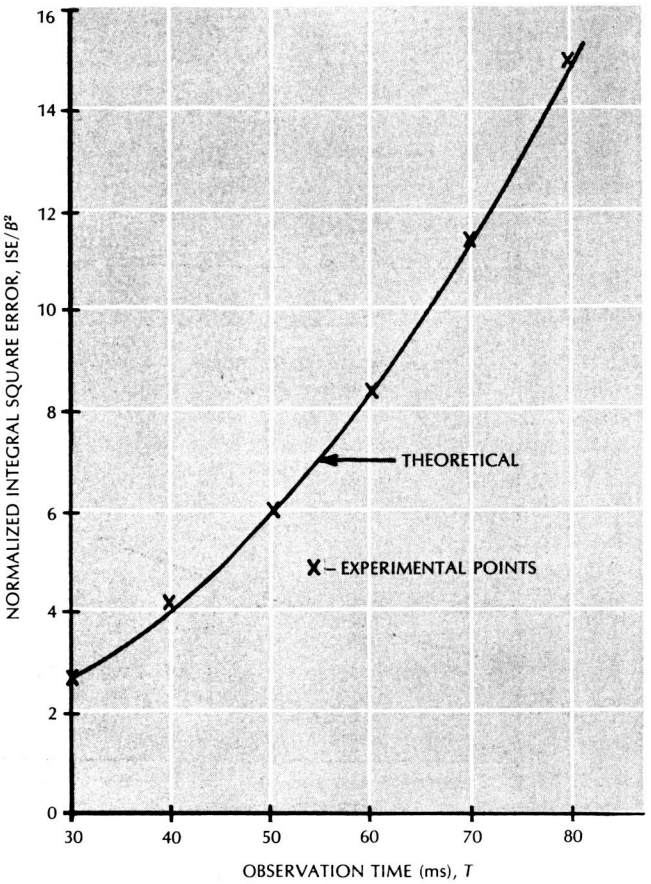

Figure 13 – Variation of Normalized Integral Square Error as a Function of Observation Time for a Constant Prediction Time of 10 ms

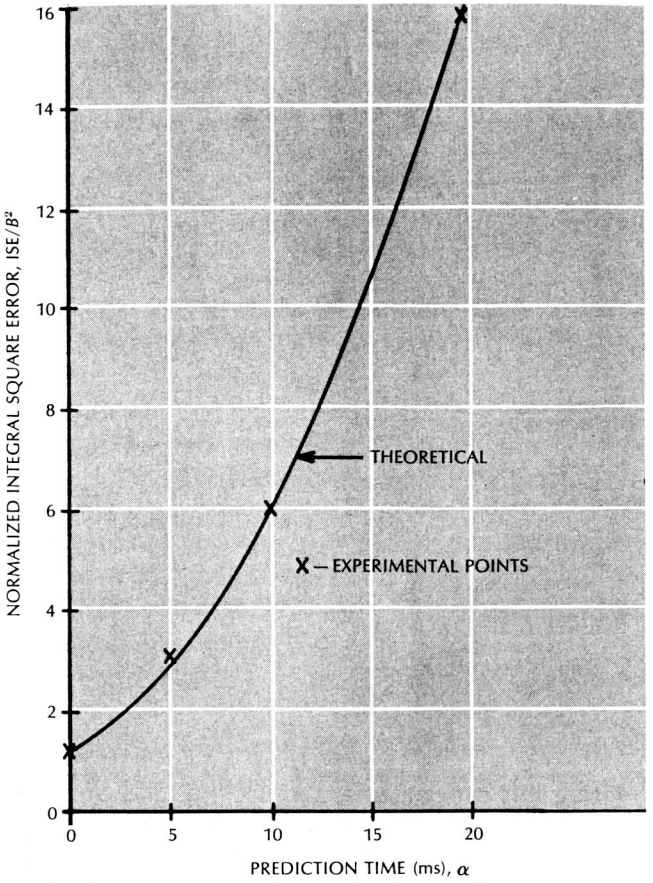

Figure 14 – Variation of Normalized Integral Square Error as a Function of Prediction Time for a Constant Observation Time of 50 ms

CONCLUSIONS

This paper has presented an iterative-differential-analyzer method for studying prediction networks. The method involves using digitally timed track-hold circuits as time delay elements. Experimental results are presented for a Wiener prediction filter and a finite-time-finite-order prediction system. These results agree very closely with the theoretical values thus verifying the method.

It should be noted that although simple examples are presented here, the method applies equally well to both nonlinear and time-varying systems.

ACKNOWLEDGMENTS

The authors are indebted to Professor Granino A. Korn of the University of Arizona, Department of Electrical Engineering, who originally suggested this project and whose many suggestions were essential to its completion.

REFERENCES

1. Korn, G. A., *New High-Speed Analog and Analog-Digital Computing Techniques:* The ASTRAC System, Electronic Industries, July 1962.
2. Bates, M. R., *et al., Analog Computer Applications in Predictor Design,* Trans. IRE/PGEC, September 1957.
3. Becker, C. L. and Wait, J. V., *Two-Level Correlation of an Analog Computer,* Trans. IRE/PGEC, December 1961.
4. Conant, B., *A Hybrid Analog-Digital Statistics Computer,* ACL Memo No. 45, Electrical Engineering Dept., University of Arizona, Tucson, Arizona.
5. Zadeh, L. A. and Ragazzini, *An Extension of Wiener's Theory of Prediction,* J. Appl. Physics, Vol. 21, pp. 645-655, July 1950.
6. Chang, S. S. L., *Synthesis of Optimum Control Systems,* McGraw-Hill, New York, N.Y., 1961, pp. 100-125.

A Simple First-order-hold Circuit

by GRANINO A. KORN
Analog/Hybrid Computer Laboratory
University of Arizona

The circuit shown in the figure converts a conventional sample-hold integrator into a first-order-hold circuit which is very useful for extrapolation of sampled data from digital-to-analog converters, multiplexers, switched-capacitor time-delay simulators, and iterative-analog-computer outputs. This circuit is an improvement over an earlier extrapolator described by L. Lofgren[1] in that the phase inverter is a-c coupled, making it possible to use a low-cost unstabilized amplifier. The circuit was tested by Messrs. Markle and Blauvelt and found to operate satisfactorily.

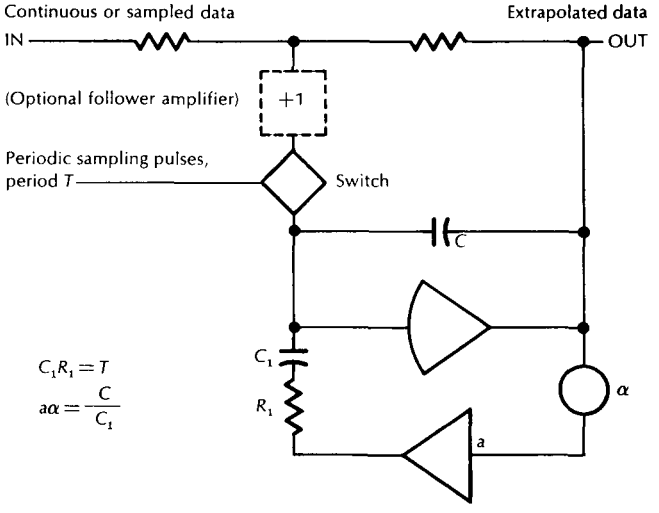

1. Lofgren, L., *Predictors in Time-shared Analog Computer*, *Proc. 1st AICA Conference*, Brussels, 1955.

DIGITAL PROGRAM CONTROL FOR ITERATIVE DIFFERENTIAL ANALYZERS

by H. R. ECKES and G. A. KORN

University of Arizona, College of Engineering
Department of Electrical Engineering
Analog/Hybrid Computer Laboratory

The following was first prepared as University of Arizona ACL (Analog/Hybrid Computer Lab) Memo No. 86. We are indebted to the authors and to the University of Arizona for permission to present this original publication.

ABSTRACT

This report identifies the timing pulses and sequential digital logic needed for practical control of iterative-differential-analyzer programs and proposes a systematic notation. Against this background, the design of a very flexible and convenient digital control unit developed for the University of Arizona's new ASTRAC II, an all-solid-state machine employing both "fast" ±10-volt amplifiers capable of iteration rates up to 1 Kc and "slow" ±100-volt amplifiers. A variety of "packaged" iteration routines is produced with a minimum of digital-logic patching. Digital-clock circuits can, in particular, control statistical evaluation of thousands of Monte-Carlo-type random-process simulations with automatic parameter changes, and will also control displays or analog-digital linkages.

ITERATIVE-DIFFERENTIAL-ANALYZER PROGRAMS

An analog computer with integrator-mode and program switches operable by sequence-controlling timers, analog comparators, and/or digital logic will be called an *iterative differential analyzer.** Such machines can automatically perform successive analog-computer runs utilizing stored results of earlier runs and can, therefore, implement iterative computations converging to a desired solution. The automatic programming features have many other applications as well.

*This term was, to the best of our knowledge, first suggested by Dr. M. Gilliland in Ref. 1 and appears to be in general use. The corresponding initials IDA, however, are a registered trademark of Beckman Instruments, Inc., and refer to their specific product.

Iterative differential analyzers, like digital computers, are programmed through a series of subroutines. A *subroutine* is a sequence of operations, such as an analog-computer run or a number of repetitive-analog-computer runs. We associate each subroutine with a digital (binary) *control variable* U_i representing the state of a control relay or flip-flop. The subroutine proceeds when $U_i = 1$; $U_i = 0$ "resets" the computing elements involved in the subroutine (e.g., integrators, counters) for renewed use. Note that the complementary control variable $\bar{U}_i$ (0 for $U_i = 1$, 1 for $U_i = 0$) may also define a subroutine. Subroutines may be "nested," *i.e.*, they may involve component subroutines.

Typical *analog-subroutine* changes are combinations of the following operations:

1. *Switching a group of integrators* from RESET to COMPUTE, or from RESET (TRACK) to HOLD, and vice versa (complementary subroutines)
2. *Switching to new values of parameter or initial-value settings* (e.g., parameter optimization, automatic scale-factor changes)
3. *Switching interconnections* to produce computer-setup changes

Subroutines start and terminate when the corresponding binary control variables change state as logical functions of (1) *external control* (switches, relays controlled by external devices), (2) *the states of timers or subroutine counters,* and (3) *analog-comparator decisions.* Appropriate Boolean functions and sequences of such control inputs can be implemented by patched digital logic.

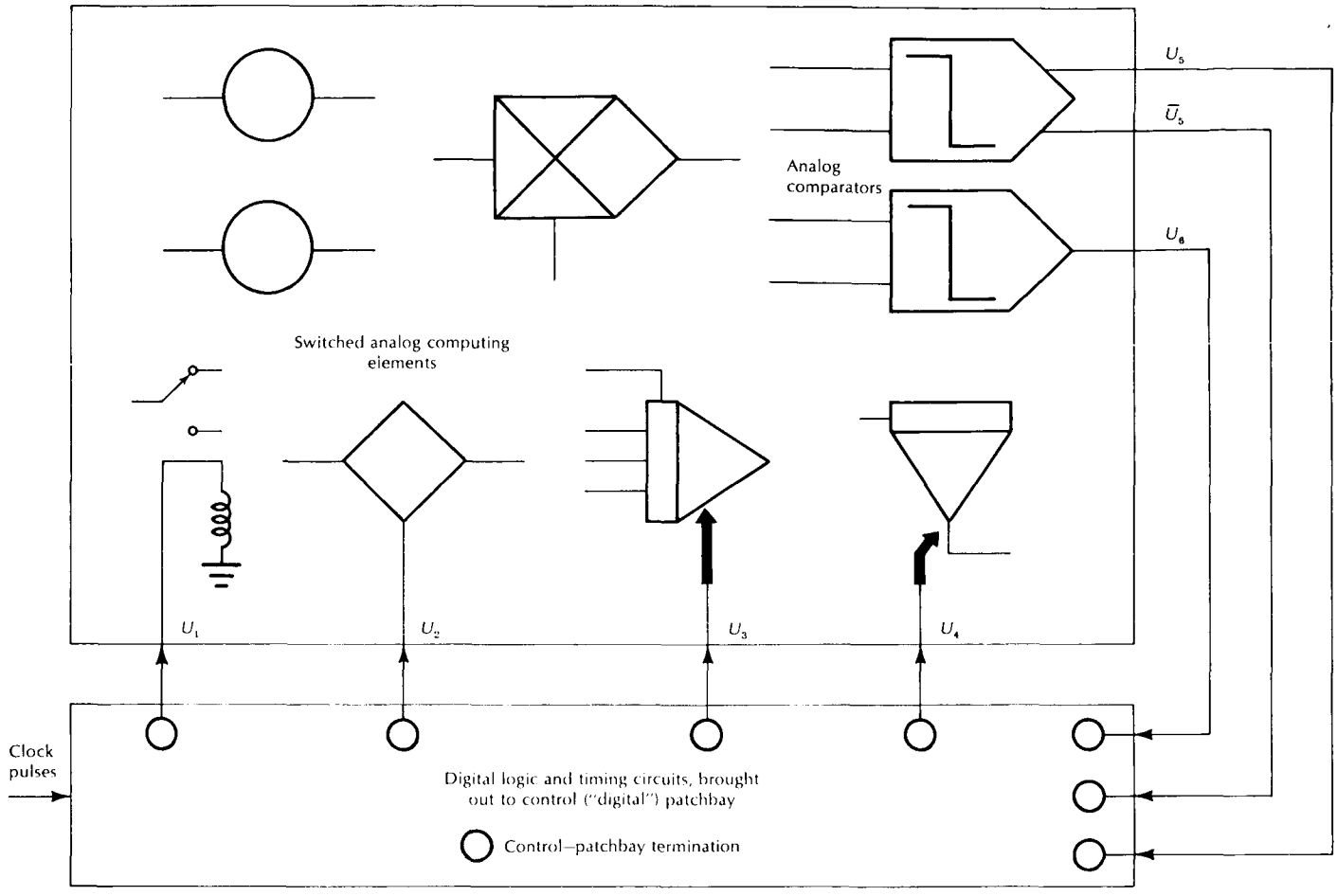

Figure 1 — Iterative-differential-analyzer system.

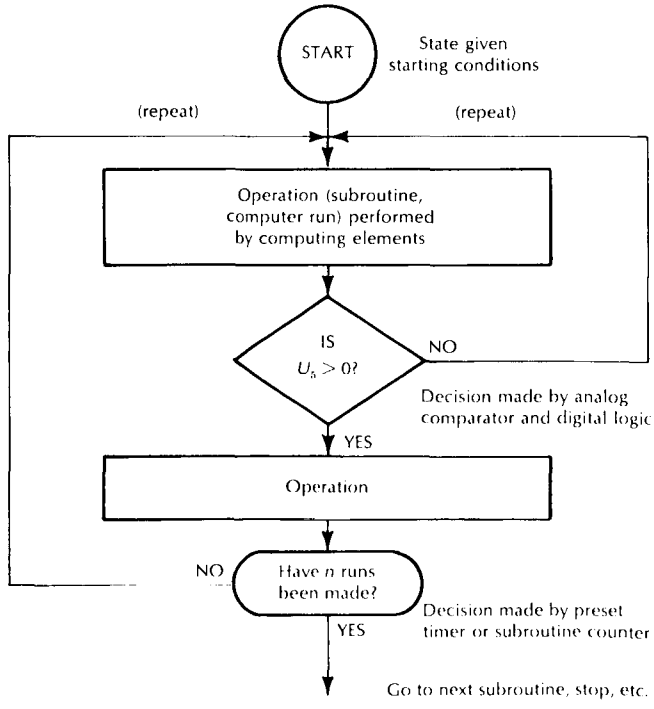

Figure 2 — Iterative-differential-analyzer flow chart. Rectangular boxes specify operations. Oval decision boxes refer to preset digital-timer and/or counter decisions, while diamond-shaped decision boxes involve analog comparators and/or comparator-actuated digital logic.

The interplay of binary control variables and analog computation gives the iterative differential analyzer a special hybrid analog-digital structure (Figure 1). Because relays or electronic switches implement analog-subroutine changes under control of digital (binary) control variables U_i, they constitute the digital-to-analog interface of our hybrid computer. Analog solutions, in turn, can modify digital controls. Program sequences of differential-analyzer operations and analog/digital decisions are nicely represented by *flow diagrams* quite similar to those used in digital computation (Figure 2).

A REVIEW OF APPLICATIONS

Iterative differential analyzers can implement vastly more sophisticated models than ordinary analog computers and still retain some of the intuitive appeal of the latter. We start our list of applications with those most peculiarly suited to iterative analog computation.

1. *Iterative Parameter Optimization.*[2 to 5] The machine varies parameters of a simulated system so as to improve performance measured in successive computer runs.
2. *Monte-Carlo Studies of Random Processes.*[2,6,7] The computer measures statistics over many fast-time computer runs simulating control systems, communication, detection, or queuing problems with random inputs.
3. *Real-time and Fast-time Simulation of Sampled-data Systems,* including digital computers.[2,8,9]

Repetitive analog computation at the highest possible speed is practically indispensable for Monte-Carlo studies of dynamical systems. Parameter optimization benefits most from high computing speed if we are required to *track* optimum-parameter combinations under changing conditions, as in cross-plotting studies or two-time-scale control.

Other interesting applications include:[2]

4. *Approximate solution of partial differential equations.*
5. *Automatic sequencing* of routine computations for plotting families of curves, special displays, cross-plotting, etc.
6. *Introduction of artificial errors* into alternate computer runs for purposes of error analysis.[10]
7. *Automatic scale-factor changes.*
8. *Multiplexing expensive computing elements* or blocks of computing elements (e.g., coordinate-transformation circuits).
9. *Special simulation and data-processing circuits,* e.g., patchbay-assembled time-division and sampling multipliers, special function generators, delays, etc.[2]

Iterative differential analyzers may also communicate with digital computers for increased accuracy and memory capacity.

BLOCK-DIAGRAM NOTATION →

Figure 3 introduces our block-diagram notation for hybrid analog-digital computer setups. Digital (binary) variables can take the *symbolic* values 0 and 1, respectively represented by deenergized and energized relays or digital-module outputs (typically 0 and −6 volts).

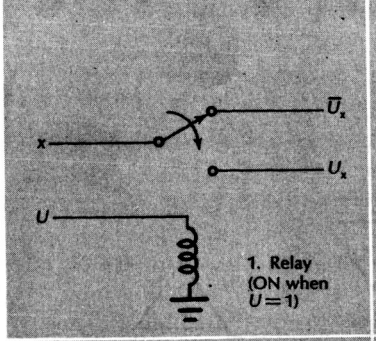

1. Relay (ON when $U=1$)

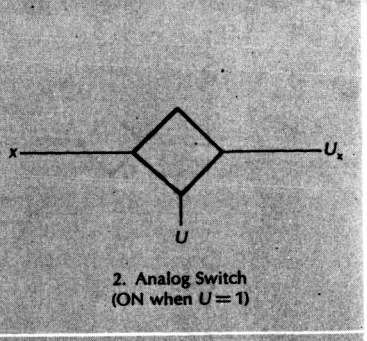

2. Analog Switch (ON when $U=1$)

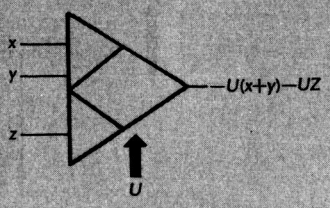

3. Switched Operational Amplifier (Lower inputs—nearest to arrow—ON when $U=1$)

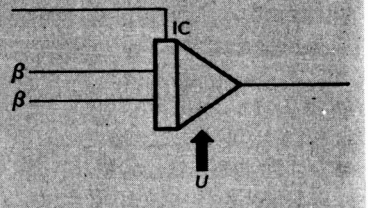

4. Two-Mode Integrator (RESET when $U=1$, COMPUTE when $U=0$)

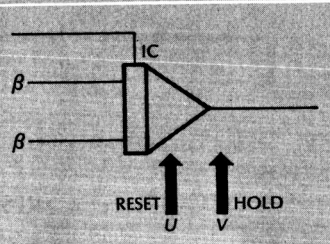

5. Three-Mode Integrator (HOLD when $V=1$, RESET when $U=1$ or $U=V=1$)

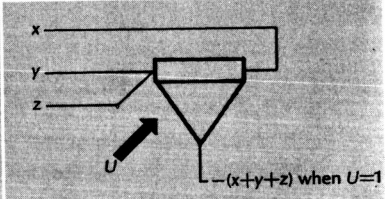

6. Track-Hold Circuit, or Integrator Used Primarily for Memory (TRACK when $U=1$, HOLD when $U=0$) *Note:* Arrow can also be *below* or *above* integrator symbol, wherever it fits best.

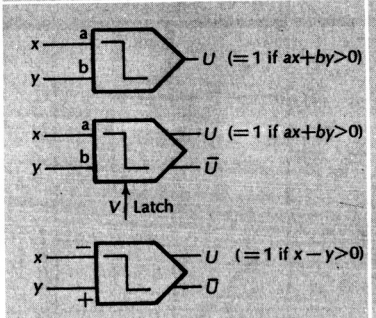

7. Analog Comparators with binary (digital) output; latch if $V=1$ (where a LATCH input is provided).

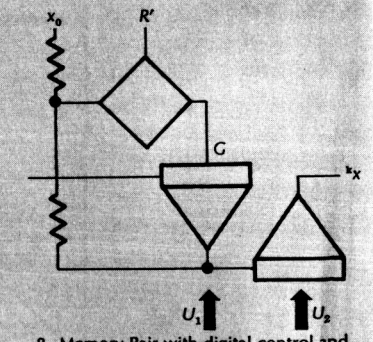

8. Memory Pair with digital control and INITIAL RESET circuit (R' is INITIAL RESET control)

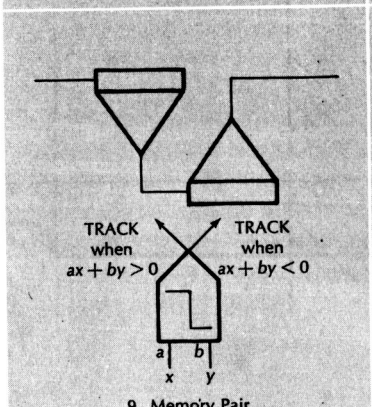

9. Memory Pair with comparator control

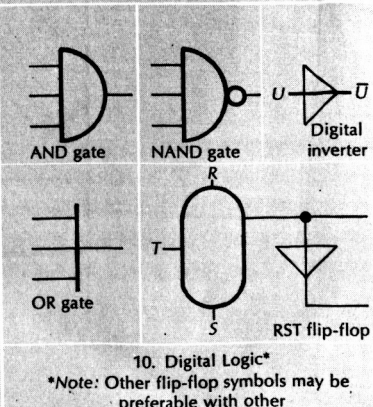

10. Digital Logic* *Note: Other flip-flop symbols may be preferable with other flip-flop types.

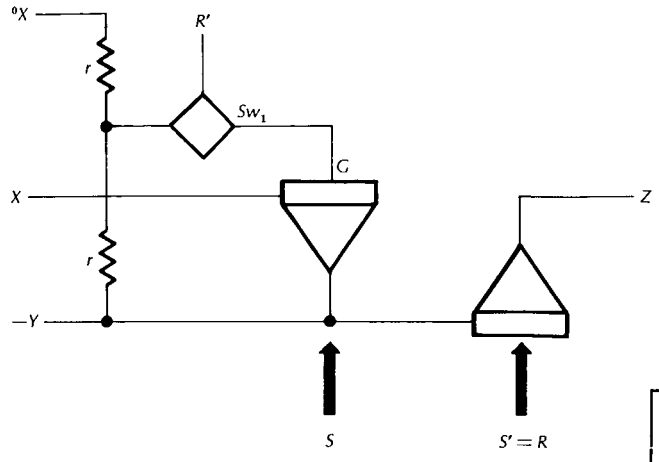

TRACK X when $R' = 0$, $S = 1$
TRACK ^0X when $R' = 1$, $S = 0$

TRACK when $R = 1$

ANALOG POINT-STORAGE OPERATION

To store the computed value $X(\tau_1)$ of an analog-computer voltage $X(\tau)$ (*point-storage*), we track $X(\tau)$ or $-X(\tau)$ with a track-hold circuit and switch into HOLD at the computer time $\tau = \tau_1 = \alpha_i t_1$. If the time derivative $PX = dX/d\tau$ is available in our computer setup, we can also store $X(\tau_1)$ by switching an integrator with input $-PX$ into HOLD.

Figure 4a — A simple memory pair can present a solution sample $^kX(\tau_1)$ during the entire following iterative-differential-analyzer run, if $\tau_1 > T_s$. Note the initial-reset-circuit operation: integrator 1 tracks the initial-reset input when $S = 0$, $R' = 1$.

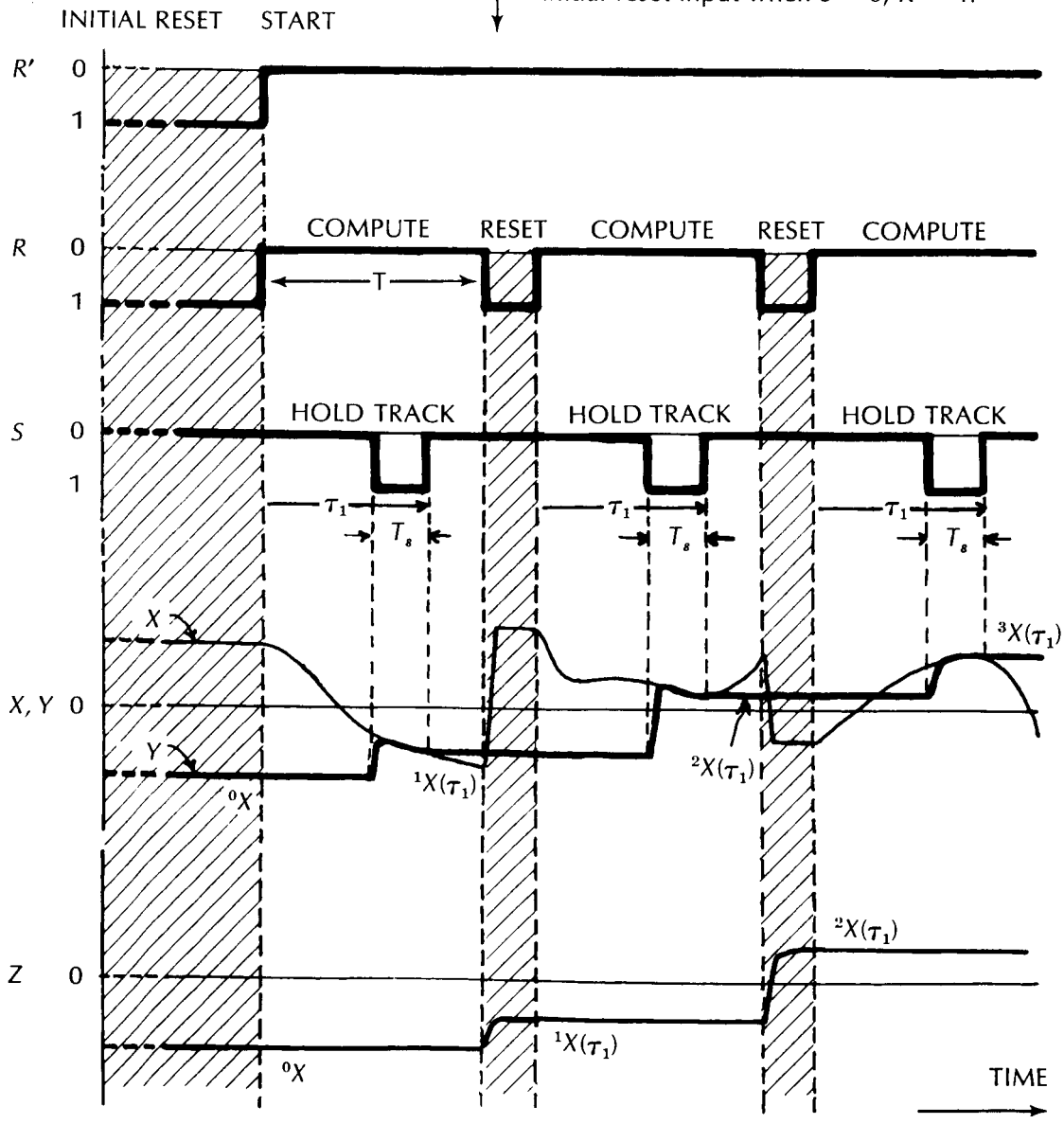

Figure 4 illustrates *memory-pair operation for information transfer between successive analog-computer runs.* In Figure 4a, the TRACK pulses $S' = R$ for track-hold 2 are delayed so that amplifier 2 tracks the HOLD output of amplifier 1 during the computer RESET period and then holds or *presents* the stored voltage during the entire subsequent COMPUTE period. Amplifier 1, in the meantime, is free to track again. Unfortunately, this scheme breaks down whenever the sampling time τ_1 is shorter than the period T_s required for tracking, for now amplifier 2 is already in HOLD at the time $\tau = \tau_1$ (Figure 4b).

There are two ways out:

1. We can interpose a third track-hold circuit between track-holds 1 and 2 to re-sample the voltage Y at a more convenient time $\tau_2 > T_s$ (Figure 4b).
2. We can use a longer computer RESET period (at least equal to $2T_s$) and switch amplifier 2 into HOLD T_s seconds after the start of the RESET period ("three-period control," Figure 4c).

Both techniques necessarily complicate our control circuits. Three-period control permits flexible operation of three-state integrators, but tends to waste possibly valuable computing time.

Frequently, a stored voltage $X(\tau_1)$ is required only during the subsequent RESET period, *e.g.*, for setting initial values or for performing an intermediate subroutine. In this case, a single track-hold circuit suffices for storage if $\tau_1 > T_s$ (Figure 4a).

THE INITIAL RESET MODE

In many applications, the memory-pair output Z in Figure 4a must assume a specified initial value ${}^0X$ during the first COMPUTE period. This is achieved by the *initial-reset circuit* shown in Figure 4a. The INITIAL RESET mode established by $R' = 1$ implies $R = 1$, $S = 0$; Sw_1 closes, and the memory output Z assumes the correct initial value $Z = {}^0X$. To start the computation, we switch to $R' = R = 0$ and let R and S cycle normally.

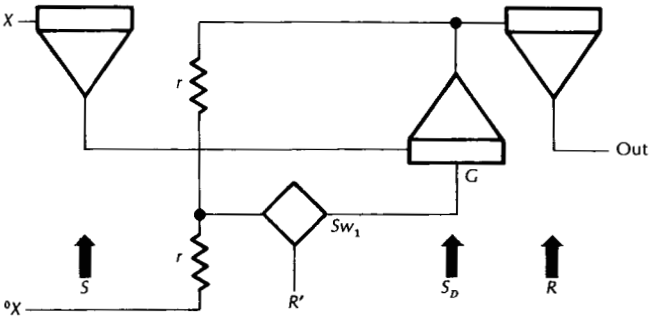

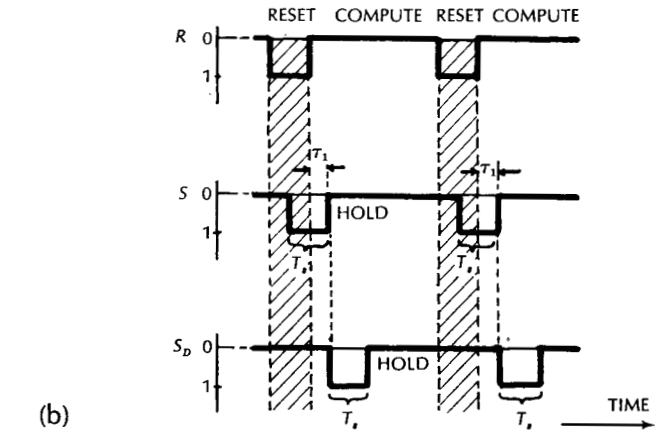

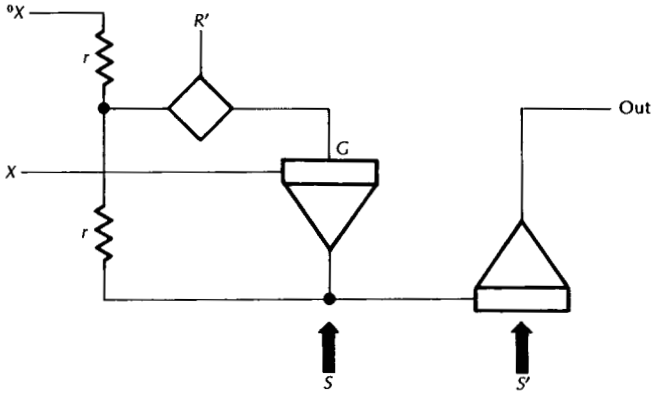

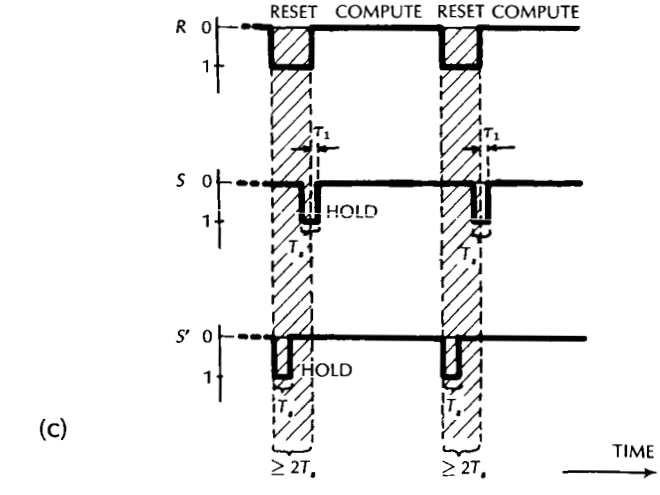

Figures 4b, c—For $\tau_1 < T_s$, the simple memory scheme of Figure 4a breaks down, since the S and R pulses overlap. To present $X(\tau_1)$ during the following computer run, we can use either an extra track-hold circuit with delayed sampling (b), or we can employ three-period control (c).

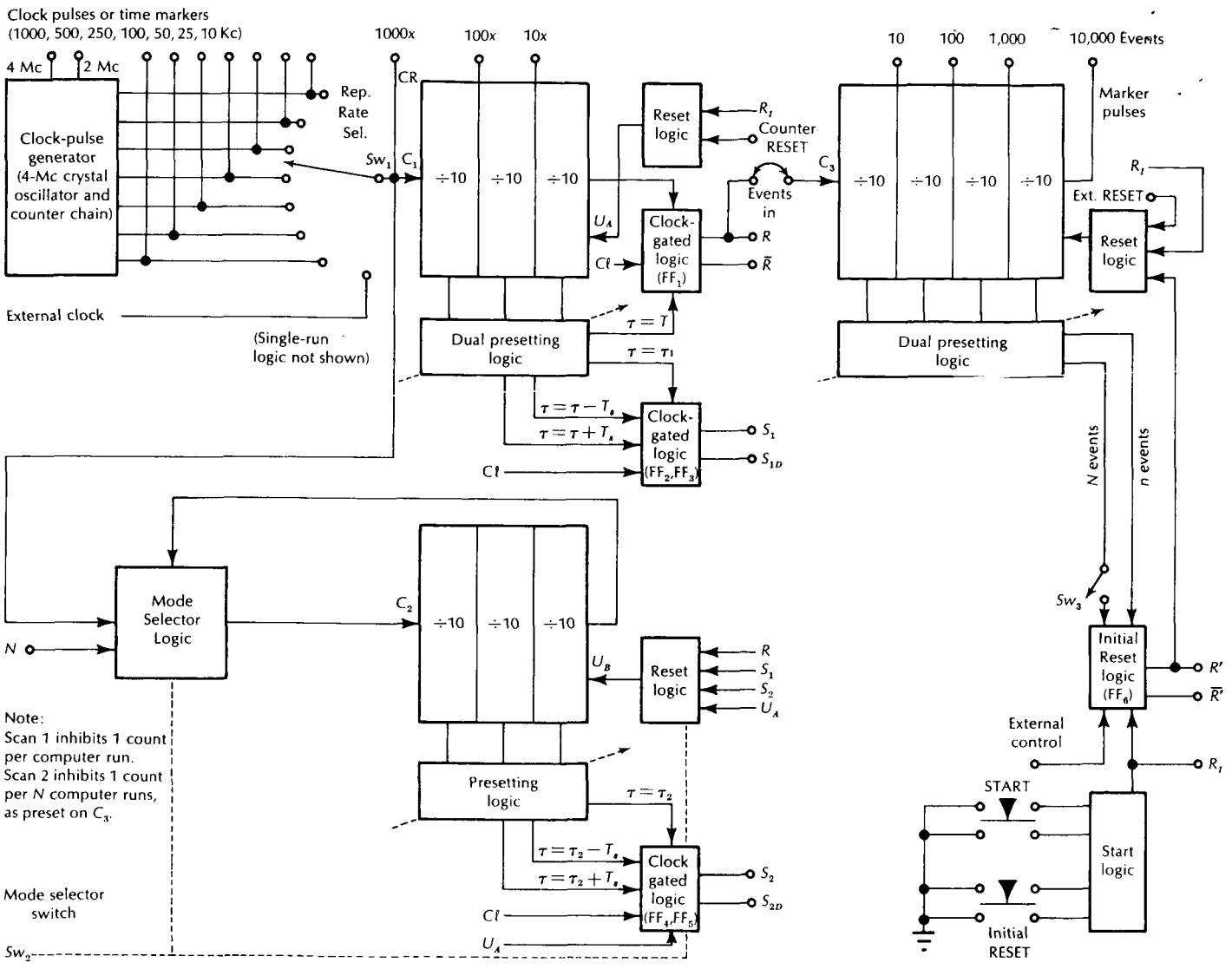

Figure 5a.—A simplified block diagram of the ASTRAC II digital iterative-differential-analyzer control unit.

DESIGN OF A DIGITAL CONTROL UNIT

Requirements

The simplest type of iterative-differential-analyzer control involves merely a source of repetitive RESET pulses, such as a simple astable multivibrator. All other subroutine control operations can, in principle, be relegated to patched digital logic.

In our judgment, though, oversimplified control circuits constitute a false economy. First, accurate repetitive computation requires stable timing to prevent synchronization of the repetition rate with the power-line frequency. Such synchronization tends to cause systematic errors, even though it makes oscilloscope displays in cheap computers look "clean," *i.e.*, free from line-frequency jitter. Timing pulses are best obtained from a simple crystal-controlled digital clock, which will also pay for itself as a source of reliable timing pulses for memory control, digital logic, oscilloscope displays, etc.

The adition of simple logic circuits to the basic digital clock can, next, produce the most frequently useful subroutine sequences with little or no digital-circuit patching. This opens the iterative technique to a much wider class of operators, for detailed iterative-subroutine design is *far from easy* for most analog-computer users. With a neat compromise between control-unit sophistication and complexity, important "packaged" subroutines can be selected by switching. Less frequently employed subroutine sequences can, of course, still be patched on a digital patchbay or pinboard adjacent to our digital control unit.

Figure 5a illustrates the design of a very flexible iterative-differential-analyzer control unit built from commercially available logic cards. Control functions are divided among a *master timer* and an *auxiliary timer* built with 5-Mc logic modules to minimize timing errors and a *subroutine counter* or counters using inexpensive 200-Kc logic. Modular design per-

mits us to start with the master timer and to add other functions as needed.

Basic Clock and Sample Timer

Referring to Figure 5a, we begin with a 4-Mc crystal clock and count down to obtain *timing pulses* for various control and display purposes. 4-Mc, 2-Mc, 1-Mc, and 500-Kc clock pulses are always available, and the repetition-rate selector Sw_1 selects clock pulses $C\ell$ at exactly 1,000 times the desired computer repetition rate $f_R = 1/T_R = 1{,}000$, 500, 250, 100, 50, 25, or 10 computer runs per second. All further timing is performed in terms of these $C\ell$ pulses (1,000 per computer run), so that the repetition-rate selector automatically changes the time scale of all timing and counting operations. If desired, the repetition-rate selector can also change integrator capacitors through relays to provide completely automatic time-scale changes.

The *master timing counter* C_1 fed by Sw_1 is a three-decade dual-preset decimal counter designed to perform the following timing functions:

1. It counts down by 1,000 to mark the start of periodic COMPUTE periods ($\tau = 0$, Figure 5b).
2. It produces timing markers at 10 times and 100 times the computer repetition rate (*e.g.*, for oscilloscope displays).
3. Thumbwheel decade switches select preset-counter outputs $\tau = T$ and $\tau = \tau_1$ seconds after the start of each COMPUTE period in steps of $T_R/1{,}000$ seconds (Figure 5b).

In normal repetitive operation (Figure 5b) flip-flop FF1 is reset at $\tau = 0$ and set at $\tau = T$ to produce periodic computer RESET pulses R, so that COMPUTE periods of length T alternate with RESET periods of length $T_R - T$. Note that we can independently select $T_R = 1/f_R$ and T. The preset output at τ_1 feeds a two-flip-flop timing-logic block to produce periodic track-hold control pulses S_1 and delayed pulses S_{1D} of length $T_S = T_R/10$. A track-hold circuit controlled by S_1 will periodically track for T_S seconds and switch into HOLD at $\tau = \tau_1$. S_{1D} switches T_S seconds later than S_1 for memory-triplet operation (Figure 4c).

All timing pulses, reset pulses, and track-hold control pulses are available in a small *control-variable patchbay* for flexible control of individual integrators and switches (Figure 6). In normal repetitive-computer operation, integrators are controlled by R, and a track-hold circuit is controlled by S_1 for digital readout of solution values $X(\tau_1)$ at the accurately preset computer time τ_1. Different patching connections can employ R, S_1, and S_{1D} to produce flexible memory control, including three-period control.

The patchable COUNTER RESET input to C_1 resets the counter to $0.9T_R$ and permits finer control of the

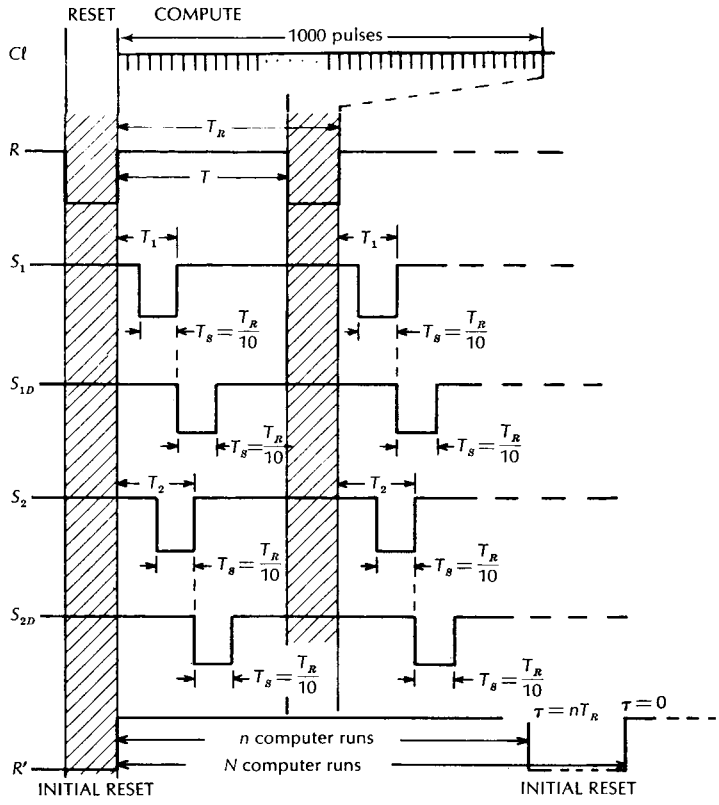

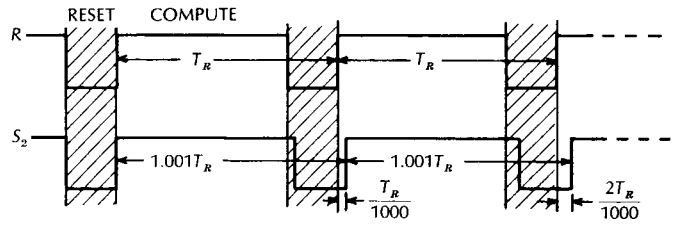

Figures 5b, c—ASTRAC II timing

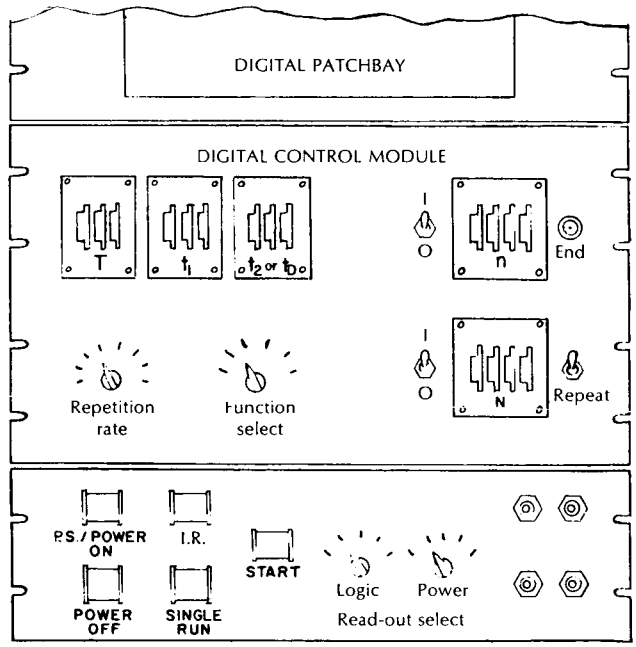

Figure 6—ASTRAC II control panel

computer-run period than is possible by repetition-rate selection. We can, for instance, use S_1 to reset the counter at $\tau = \tau_1$; this will reset integrators for 0.1 $T_R = T_S$ seconds and then start a new COMPUTE period of duration τ_1. Many other possibilities exist; it is, in particular, possible to control the lengths of individual computer runs with patched comparator logic to conserve time in long computations.

Auxiliary Timer and Scan Readout

The auxiliary *timing counter* C_2 in Figure 5a is another three-decade preset counter. With its associated logic circuits, C_2 adds the following functions to the basic clock:

1. With switch Sw_2 in the "τ_2" position, C_2 produces a preset output τ_2 seconds after the start of each COMPUTE period. Logic circuits yield track-hold control pulses S_2 and S_{2D} analogous to S_1 and S_{1D}.
2. With Sw_2 in the "τ_D" position, C_2 is reset periodically at $\tau = \tau_1$. The timing pulses switching S_2 to 0 (HOLD) occur at $\tau = \tau_1 + \tau_D$, with thumbwheel-preset on C_1 and C_2. This produces, in particular, sample pairs $X(\tau_1)$, $Y(\tau + \tau_D)$ for correlation and prediction studies.
3. With Sw_2 in the "T" position, C_2 is reset at $\tau = T$, and S_2, S_{2D} serve for readout during the RESET period just as S_1, S_{1D} serve during the COMPUTE period. This is useful for "alternating" differential-analyzer runs using integrator groups controlled by R and R and also permits flexible three-period control.
4. With Sw_2 in the "SCAN 1" position, C_2 recycles after 1,001 input pulses. With C_1 and C_2 initially reset to 0.9 T_R and zero, and C_2 preset to T_R/1,000 sec, S_2 will read out at $\tau_2 = T_R$/1,000 sec during the first computer run, at $\tau_2 = 2T_R$/1,000 sec during the second computer run, etc. (Figure 5c). *Track-hold circuits controlled by S_2 and S_{2D} will then "scan" periodic repetitive-computer solutions once every 1,000 computer runs for readout into slow recorders, printers, or digital computers.* With $f_R = 100$ cps, for instance, a complete scan requires 10 seconds.
5. With Sw_2 in the "SCAN 2" position, the subroutine counter permits the scan to step forward only after a preset number N of computer runs or other events.
6. With Sw_2 in the "REVERSE SCAN" position, C_2 resets after between 500 and 1,000 input pulses. Wtih C_1 and C_2 initially reset to zero and C_2 preset to mT_R/1,000 sec, τ_2 starts at that time and scans *backwards* in steps of $(1 - m/1{,}000)$ T_R sec per computer run.

The SCAN modes are useful for slow recording of repetitive solutions (X *vs.* τ or Y *vs.* X), but also for automatic parameter changing (new values of a repetitive solution $X(\tau)$ are used in successive computer runs), for multiple-solution oscilloscope displays, and for solution checks with slow computers. The "REVERSE SCAN" mode, with its wide choice of scanning rates, is useful for computing convolution integrals, for backward integration (*e.g.*, in boundary-value problems), for modified-adjoint-system techniques, and for controlling delay-line-memory read/write cycles. The "SCAN 2" mode is intended for automatic computation of statistics over n computer runs.

Subroutine Counter and Repeat Switch

Referring again to Figure 5a, the *subroutine counter* C_3, another dual-preset 4-decade counter, is patched to count computer runs, comparator-output steps, or other events. C_3 produces output pulses every 10, 100, 1,000, and 10,000 events, as well as preset-counter outputs after n and N events ($n, N < 20{,}000$). These counter outputs are used to terminate and/or start subroutine sequences. In particular, the REPEAT switch Sw_3 permits us to reset C_3 to zero after N events and to recycle the sequence.

Starting, Two-Time-Scale Operation, and External Control

Before computation, we depress the *INITIAL RESET* button momentarily or hold the start button down (Figure 5a) to produce the following conditions:

1. The subroutine counter C_3 is reset to zero and establishes the INTIAL RESET mode ($R' = 0$).
2. The main timing counter C_1 is reset to $T_R - T_S = 0.9T_R$; flip-flops FF1 to FF4 are set or reset to produce $R = 1$ and correct initial values of the control variables S_1, S_{1D}, S_2, and S_{2D}. C_2 are reset to zero, except in the "τ_D" mode, where it is reset to T_R/1,000.
3. In any SCAN mode, counter C_2 is reset to zero.

It follows that all integrators, memory pairs, and statistical averaging devices controlled by R and R' are now reset to suitable initial conditions, ready for computation.

This state is maintained until we release (or depress and release), the *START button* momentarily. Then C_1 runs through 100 $C\ell$ pulses (T_S seconds) and then starts the first COMPUTE period (see also Figure 4a). To produce "nested" iterative subroutines, the REPEAT switch Sw_3 reestablishes the INITIAL RESET mode ($R' = 1$) after a preset number n of subroutine-counter input pulses, and resets the subroutine counter after $N > n$ pulses to repeat the cycle (Figure 5b). In particular, we can reset fast integrators with R and slow integrators with R' (*two-time-scale operation*).

If the *SINGLE-RUN switch* Sw_4 is closed, then the *SINGLE-RUN button* produces a single computer run ($R = 0$) without resetting C_1, C_2, or C_3, so that we can check the progress of iterative subroutines, computer run by computer run. The various resetting, sampling, and starting operations can also be ordered electronically by external command pulses into appropriate lines.

Physical Construction

Computer Control Company, Inc. S-PAC NAND logic and gated flip-flops are used throughout the digital control unit. Wire-wrap connections to the control unit and to the digital control patchbay (VECTOR PPB 600A) simplify construction and simplify circuit changes.

The basic clock uses 5-Mc logic and consists of a 4-Mc crystal-controlled oscillator, two flip-flops, and two decade counters, producing 4 Mc, 2 Mc, and 1,000 f_r waveforms. The 4-Mc signal also serves as the clock for a Hybrid Analog-Digital Random-Noise Generator.[12] The 2-Mc signal is the clock for a hybrid analog-digital delay system.[13,14] The remaining signals trigger C_1 and C_2 logic.

C_1 and C_2 counters and their logic circuits also use 5-Mc logic to keep the ripple-through timing error well below 1 μsec, allowing the output flip-flops to be clocked by 1000 $f_r \leq 1$ Mc. Clocking eliminates timing errors in the outputs of the control unit.

C_3 counters use inexpensive 200-Kc logic, because the fastest input signal is $f_r \leq 1$ Kc. The output logic is clocked by the input to C_3 to eliminate timing errors.

All outputs of the control unit are isolated by power amplifiers before being brought out to the digital control patchbay.

The complete logic diagram for the control unit is available on request to the authors.

ACKNOWLEDGMENT

The project described in this report is part of a hybrid analog-digital computer study directed by Professor G. A. Korn. The writers are very grateful to the Office of Aerospace Research, Information Research Division, Air Force Office of Scientific Research and to the Office of Space Sciences, National Aeronautics and Space Administration for their continuing support of this study under joint grant AF-AFOSR-89-63; and to Drs. T. L. Martin, former Dean of Engineering, and P. E. Russell, former Head of Electrical Engineering Department; and Professor L. Matsch, Acting Dean of Engineering, and Professor Harry Stewart, Acting Head of Electrical Engineering, for their encouragement and contribution of University facilities.

REFERENCES

1. Gilliland, M. C., Iterative Differential Analyzer Function and Control, *Instruments and Control Systems*, April, 1961.
2. Korn, G. A., and T. M. Korn, *Electronic Analog and Hybrid Computers*, McGraw-Hill, N.Y., 1964 (in print).
3. Stakhovskii, R. I., Development and Investigation of an Automatic Optimizer, *Automatika i Telemekhanika*, August, 1958.
4. Witsenhausen, R., Hybrid Techniques Applied to Optimization Problems, *Proc. SJCC*, 1962, and *SIMULATION*, Fall, 1963.
5. Mitchell, B. A., Hybrid Analog-digital Parameter Optimizer for ASTRAC II, MS Thesis, University of Arizona, 1964 (in preparation).
6. Korn, G. A., New High-speed Analog and Analog-digital Computing Techniques: The ASTRAC System, *Proc. 3rd AICA Conference*, Opatija, Yugoslavia, 1961; Presses Academiques Europeennes, Brussels, 1962; see also *Electronic Industries*, July, 1962.
7. Brubaker, T., and H. R. Eckes, Digital Control Unit for a Repetitive Analog Computer, *Proc. WJCC*, 1961.
8. Bekey, G., and W. J. Karplus, in *Lecture Notes on Hybrid Computing Techniques*, University of California, Los Angeles, 1963.
9. Reich, J. E., and J. J. Perez, Design and Development of a Sampled-data Simulator, *Proc. WJCC*, 1961.
10. Korn, G. A., Parameter-perturbation Generator for Analog-computer Error and Optimization Studies, *Ann. AICA*, April, 1963.
11. *DYSTAC Applications* (Eastern Simulation Council presentation, December 12, 1960), published by Computer Systems, Inc., Fort Washington, Pa., 1960.
12. Hampton, R., G. A. Korn, and B. Mitchell, "Hybrid Analog-Digital Random-Noise Generation," *IEEE Transactions on Electronic Computers*, Aug., 1963.
13. Korn, G. A., "Analog/Hybrid Storage and Pulse Modulation," *IEEE Transactions on Electronic Computers*, Aug., 1963.
14. Handler, H., and R. Mangels, "A 2-Mc Delta-sigma Modulation System for Delay-line Function Memory," ACL Memo No. 89, Electrical Engineering Dept., University of Arizona, Tucson, Arizona, 1963.